American Journal of Applied Mathematics
2025; 13(1): 30-56
http://www.sciencepublishinggroup.com/j/ajam
doi: 10.11648/j.ajam.20251301.13
ISSN: 2330-0043 (Print); ISSN: 2330-006X (Online)

Hydromagnetic Casson Nanofluid Flow Past a Wedge in a Porous Medium in the Presence of Induced Magnetic Field

Nyaga Danson[1, *], Ochwach Jimrise[1, 2], Kirimi Jacob[1], Okongo Mark[1]

[1]Department of Physical Science, Faculty of Science and Technology, Chuka University, Chuka, Kenya
[2]Department of Computing and Information Technology, School of Pure and Applied Sciences, Mama Ngina University College, Gatundu, Kenya

Email address:

dansonnyaga@gmail.com (Nyaga Danson), h.kirimi@yahoo.com (Kirimi Jacob), ojimrise09@gmail.com (Ochwach Jimrise), Marikookongo@gmail.com (Okongo Mark)
[*]Corresponding author

To cite this article:

Nyaga Danson, Ochwach Jimrise, Kirimi Jacob, Okongo Mark. (2024). Hydromagnetic Casson Nanofluid Flow Past a Wedge in a Porous Medium in the Presence of Induced Magnetic Field. *American Journal of Applied Mathematics, 13*(1), 30-56.
https://doi.org/10.11648/j.ajam.20251301.13

Received: 19 September 2024; **Accepted:** 8 October 2024; **Published:** 20 January 2025

Abstract: Casson fluid is a shear thinning liquid assumed to have an infinite viscosity at zero rate of shear and a zero viscosity at an infinite rate of shear. Casson fluids at times flow past wedge-shaped objects, as is the case in crude oil extraction and geothermal systems. Nanoparticles tend to improve thermal conductivity of base fluids. The impact of Magnetohydromagnetics (MHD) and induced magnetic field on heat and mass transfer flow finds application in engineering and industries. It plays an important role in design of transpiration cooling and aerodynamics extrusion of plastic sheets. Several authors have studied effects of induced magnetic field on different types of fluid flow. However, little has been studied on the impact of induced magnetic field on Casson Nanofluid flow past a wedge. In this study, the equations governing the nanofluid flow were reduced to a system of highly nonlinear ordinary differential equations by using boundary layer theory. The resulting boundary value problem is then numerically solved in MATLAB by using the Boundary Value Problem 4th-order collocation (BVP4C). The local skin friction, mass transfer rate, and heat transfer rate are displayed in a table while graphs illustrate the influences of pertinent physical entities on the temperature, nanofluid velocity, concentration of nanoparticles and magnetic induction. The study's findings will improve the body of knowledge on Casson Nanofluid flow past a wedge, which is important for plasma, fossil fuels, blood flow in the circulatory system, glass fibre manufacture, petroleum production, and magma dynamics. Due to their low thermal conductivity, electrically conducting Casson fluids have rather poor heat transfer; however, thermal conductivity is improved when nanoparticles are introduced and induced magnetic fields are considered significant. As a result, manufacturers can create solutions using the findings of this study. The issues surrounding induced magnetic fields are significant in several industrial applications, including geothermal systems, liquid metals, fibre or granular insulation, electrolytes, and ionised gases.

Keywords: Casson Fluid, Nanofluid, Hydromagnetic, Induced Magnetic Field, Nanoparticle

1. Introduction

Magnetohydromagnetics (MHD) is the study of the behavior of an electrically conducting fluid as it flows in the presence of a magnetic field [34]. From a technical perspective, it is crucial to investigate the flow of an electrically conducting fluid in the presence of a magnetic field. There are numerous instances where a strong magnetic field is encountered in an electrically conducting fluid. These include applications in nuclear engineering, astrophysical flows, solar power technology, electric power generation, and space vehicle re-entry, among others [2, 3, 25]. The following are some examples of applications in engineering and industry: MHD pumps, grain regression, electrostatic precipitation, aerodynamic heating, paper and textile dyeing, liquid crystal solidification, food preservation, petroleum industries, cooling of metallic sheets in baths, and magneto

hydrodynamic generators [1, 13, 40].

A fluid particle in motion experiences inertia forces, which result in zero acceleration. They are in opposition to an applied force and oppose changes in an object's speed [4, 18].

Ali *et al* [7] The Reynolds number determines how much the applied magnetic field changes as a result of induced electric currents in the flow field. When a real fluid passes a solid barrier that is stationary, the layer of fluid that touches the boundary surface has a velocity equal to the surface. In the fluid layer that can't break away from the boundary surface, retardation takes place. Because of the additional retardation that this retarded layer causes to the adjacent fluid layers, the fluid in the immediate vicinity of the boundary surface develops a small region where the velocity of the flowing fluid rapidly increases from zero at the boundary surface to the velocity of the main stream. The layer closest to the boundary is known as the boundary layer [5, 28, 33, 38].

The boundary layer may have laminar or turbulent properties, depending on the values of the Reynolds number. At lower Reynolds numbers, the boundary layer is laminar; at higher Reynolds numbers, it is turbulent.

The magnetic field's action creates a Lorentz force in the boundary layer that tends to impede the flow, preventing the fluid layer from coming into contact with the wedge wall. Less heat is transferred from the fluid to the wall as a result. This is thought to be a very significant element in giving wedge walls extra protection [8, 35].

Several factors have been studied when applying a magnetic field to control the motion of an electrically conducting fluid. These factors include the type of conducting fluid, the geometry of the flow the fluid is in, the source of the magnetic field, the fluid's degree of ionization, and the applied Magnetic field strength [12, 14]. Mccormack random molecule motion usually predominates near the surface where the fluid velocity is low, and this is typically the contribution from diffusion. The convection heat transfer method is influenced by the density, conductivity, and specific heat of the fluid. Fluid flow is impacted by viscosity. Heat transfer is widely used in many different applications, such as heat exchangers that improve heat transmission or steam pipes that try to limit it. In modern technology, heat transfer is significantly employed in areas such as energy production, nuclear reactors, and heat exchangers (which are used in power generation, air conditioning, refrigeration, and space heating) [6, 17, 20].

Murshed and Castro [29] observed that because of their poor heat transfer qualities, conventional heat transfer fluids including water, ethylene glycol, and engine oil have restricted heat transmission capabilities. It is naturally desired to combine the two materials to create a heat transfer medium that behaves like a fluid but has the thermal properties of a metal because metals have thermal conductivities that can be up to three times higher than those of these fluids.

Percy *et al* [51] observed that the transportation industry (cars, trucks, and airplanes), industrial cooling applications, nuclear reactors, micro-electromechanical systems (MEMS), electronics, and instrumentation, as well as biomedical applications like nano-drug delivery, cancer therapeutics, and cryopreservation, could all benefit from the novel class of heat transfer fluids known as nanofluid [41, 42]. Heat transfer is the movement of thermal energy between physical systems. The rate of heat transmission depends on the system temperature and the properties of the medium. On the other hand, temperature is the result of using a thermometer to quantify hotness or coolness. Variations in temperature inside a fluid can be caused by differences in temperature between the fluid at the boundary and the ambient fluid [32, 36, 50].

The absorption of thermal energy across a boundary in a thermodynamic system is another source of variance. As a result, by dissipating heat, heat transfer - which defines the flow of thermal energy between physical systems - depends on temperature and pressure [23, 24].

According to Singh and Myong [43], the three less complex processes that make up heat transmission are radiation, convection, and conduction. The laws that govern each of these heat transfer methods are different [16, 26, 30]. The process of molecular heat transfer by tiny particles (atoms, molecules, ions, etc.) in a medium with a temperature gradient is known as conduction of heat. Heat is transferred through convection, which is the movement of a medium's macroscopic components, also known as molar volumes [48–50]. Convective heat transfer is the process that transfers heat when heat conduction and convection occur simultaneously. The particular instance of this process is convective heat exchange, or heat transfer, which occurs between a moving media and its interface with a solid, liquid, or gaseous medium [22, 31].

Heat transfer modifies the internal energy of both participating systems, in accordance with the first rule of thermodynamics. Measurable heat transfer is how the second law characterizes thermodynamics. An equilibrium state is reached when all bodies are at the same temperature. The geometrical, hydrodynamic, and thermal properties of the system under examination all affect the heat transfer coefficient, which is not a constant value [44, 45].

Bachok and Ishak [9]. When flow occurs across a surface, a velocity boundary layer forms. It is linked to shear forces that run parallel to the surface, and it causes the velocity to rise through the boundary layer from almost zero at the surface to the free stream velocity at a considerable distance from it.

Conventionally, the thickness of the boundary layer is determined by measuring the distance from the surface to the height above the surface at which the velocity is 0.99 of the free stream velocity [10, 46, 47].

2. Model Formulation

A steady two-dimensional, incompressible, laminar, free convective heat and mass transfer flow of a Casson Nanofluid past a stationary wedge with influence of induced magnetic field is studied.

2.1. Flow Configuration

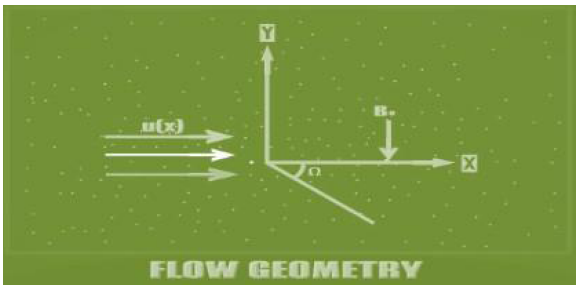

Figure 1. *Flow Configuration.*

At the wall of the wedge, $U_w(x) = 0$ for the stationary wedge and at time $t = 0$, the temperature of the wedge is T_w with species concentration C_w Instantaneously at $t > 0$, the temperature of the wedge surface and the species concentration of the wedge surface are raised to T_∞ and C_∞ respectively which are thereafter maintained constant. A strong magnetic field $\vec{\mathbf{B_0}}$ is applied in y $-$direction. The motion of fluid drags the induced magnetic field $\vec{\mathbf{b}}$ along the x$-$ axis towards the direction of fluid flow. The Lorentz force, which is created by this dragging, opposes the dragging of the magnetic field. When an electrically conducting fluid is subjected to a normal magnetic field, the Lorentz force is generated. The fluid motion is choked down by this force because it is directed against the direction of the fluid flow.

2.2. Continuity Equation

The Casson fluid flows continuously and its mass is conserved. The flow is considered as incompressible in this study. The foundation of the continuity concept consists of two fundamental propositions which are:

1. Since mass cannot be created or destroyed, the fluid's mass is conserved.
2. The flow is continuous such that there are no empty spaces in between particles in contact. The fluid element's net mass rise per unit time must be equal to the fluid element's mass increase rate.

Mass of the fluid in element is given by: $\rho(dxdydz)$
The rate of increase with time is:

$$\frac{\partial}{\partial t}(\rho dxdydz) = \frac{\partial \rho}{\partial t}(dxdydz) - \left[\frac{\partial}{\partial x}(\rho u)\frac{\partial}{\partial y}(\rho v)\frac{\partial}{\partial z}(\rho w)\right]dxdydz$$
$$= \frac{\partial \rho}{\partial t}(dxdydz)\frac{\partial \rho}{\partial t} + \frac{\partial}{\partial x}(\rho u) + \frac{\partial}{\partial y}(\rho v) + \frac{\partial}{\partial z}(\rho w) = 0 \tag{1}$$

This study is dealing with a two-dimensional steady flow, such that the density is constant and the variables are independent of time and so the equation of continuity reduces to

$$\frac{\partial u}{\partial x} + \frac{\partial v}{\partial y} = 0 \tag{2}$$

2.3. Equations of Conservation of Momentum

This equation is derived from Newton's second law of motion, which stipulates that in the context of fluid dynamics, the rate of change of total momentum in a fluid motion must equal the sum of forces acting on the fluid. It is also known as the equation of motion or Euler's equation of motion.

$$\frac{\partial \vec{q}}{\partial t} + (\vec{q}.\nabla)\vec{q} = -\frac{1}{\rho}\nabla \mathrm{P} + \vartheta \nabla^2 \vec{q} + \vec{F} \tag{3}$$

Here, $\frac{\partial \vec{q}}{\partial t}$ is the temporal acceleration
$(\vec{q}.\nabla)\vec{q}$ is the convective acceleration
$-\frac{1}{\rho}\nabla \mathrm{P}$ is the pressure gradient
$\vartheta \nabla^2 \vec{q}$ is the viscous drag
$\vec{F}$ is the external force due to gravitational field $\vec{F_g}$ and the electromagnetic force $\vec{F_e}$, where $\vec{F_e}$ is given by $\rho_e E + \vec{J} \times \vec{B}$ and $\vec{J} = \delta(\vec{E} + \vec{q} \times \vec{B})$ (Ohms law) for a moving electrically conducting fluid in a magnetic field $\vec{B}$.

Since we are dealing with laminar two-dimensional flow with pressure gradient being zero,

$$(\vec{q}.\nabla)\,\vec{q} = \vartheta \nabla^2 \vec{q} + \vec{F} \tag{4}$$

$$\vec{q} = \mathbf{u}\vec{i} + \mathbf{v}\vec{j} \tag{5}$$

Gradient operator

$$\nabla = i\frac{\partial}{\partial x} + j\frac{\partial}{\partial y} + k\frac{\partial}{\partial z} \tag{6}$$

$$(\vec{q}.\nabla)\,\vec{q} = (ui + vj).(i\frac{\partial}{\partial x} + j\frac{\partial}{\partial y} + k\frac{\partial}{\partial z})(\,ui + vj) = u\frac{\partial}{\partial x} + v\frac{\partial}{\partial y} \tag{7}$$

$$\vartheta \nabla^2 \vec{q} = \vartheta(\frac{\partial^2}{\partial x^2} + \frac{\partial^2}{\partial y^2})\,(ui + vj) \tag{8}$$

This work addresses the heat and mass transfer of a Casson nanofluid embedded in a porous medium with viscous dissipation, Brownian motion, and thermophoresis parameter effects in MHD boundary layer flow past a wedge. The Hartree pressure gradient parameter related to the wedge total angle Ω and the Falkner-Skan power-law parameter is m and β whose relation is: $\beta = \frac{2m}{1+m}$ and $\beta = \frac{\Omega}{\Pi}$.

For the stationary wedge with wedge angle Ω, the momentum equation is therefore written as:

$$\mathbf{u}\frac{\partial u}{\partial x}+\mathbf{v}\frac{\partial u}{\partial y}=U_{\mathbf{x}}\frac{du}{dx}+\vartheta(1+\frac{1}{\beta})(\frac{\partial^2 u}{\partial x^2}+\frac{\partial^2 u}{\partial y^2})+\vec{F} \quad (9)$$

The Lorentz forces $\vec{F}$ are produced by a strong applied magnetic field combined with an induced magnetic field. These can be obtained using the equations of Maxwel. The flow incorporates Maxwell's electromagnetism equations since it is subjected to a strong applied magnetic field.

$$\nabla \times E=-\frac{\partial B}{\partial t} \quad (10)$$

With the assumption of absence of external electric field, E=0.

The total electromagnetic force Fe=$J \times B$ where

$$J=\sigma\left(E+q\times B\right) \quad (11)$$

but E=0 and

$$\vec{\mathbf{B}}=\vec{\mathbf{b}}i+\vec{\mathbf{B}}_{\mathbf{0}}j \quad (12)$$

$$\mathbf{q}\times\mathbf{B}=\begin{vmatrix} i & j & k \\ u & v & 0 \\ b & B_0 & 0 \end{vmatrix}=\mathbf{uB_0k}-\mathbf{bvk} \quad (13)$$

$$\mathbf{J}\times\mathbf{B}=\begin{vmatrix} i & j & k \\ 0 & 0 & \mathbf{uB_0}-\mathbf{bv} \\ b & B_0 & 0 \end{vmatrix}=(-\mathbf{uB_0^2}+\mathbf{B_0bv})i \quad (14)$$

The specific momentum equation governing the flow, considering electrical conductivity σ in x-direction is:

$$u\frac{\partial u}{\partial x}+v\frac{\partial u}{\partial y}=U(\infty)\frac{du_\infty}{dx}+\vartheta(1+\frac{1}{\beta})(\frac{\partial^2 u}{\partial x^2}+\frac{\partial^2 u}{\partial y^2})-\frac{\sigma B_0^2(u-u_\infty)}{\rho}+\frac{\sigma B_0 bv}{\rho} \quad (15)$$

2.4. The Magnetic Induction Equation

$$\frac{\partial B}{\partial t}=\vec{\nabla}\times(\vec{q}\times\vec{B})+\frac{1}{\mu_0\sigma}\vec{\nabla}^2\vec{B}$$

$$\eta_0=\frac{1}{\mu_0\sigma}$$

The magnetic induction equation is derived by taking the curl of Ohms law.

$$\vec{\nabla}\times\frac{\vec{j}}{\sigma}=\vec{\nabla}\times\tilde{\mathbf{E}}+\vec{\nabla}\times(\tilde{\mathbf{q}}\times\tilde{\mathbf{B}}) \quad (16)$$

This is the general induction equation, which suggests that the motion of a conducting liquid in an applied magnetic field will induce a magnetic field in the medium. $\vec{B}=B_0+\mathbf{b}$ is the total magnetic field which is the sum of the applied magnetic field B_0 and the induced magnetic field $\mathbf{b}$. For our case, we first make $\mathbf{J}$ the subject of the formula in the Ampere' s equation of electromagnetic induction $\vec{\nabla}\times\vec{B}=\mu_0\vec{J}$

$$\vec{J}=\frac{\nabla\times\vec{B}}{\mu_0}$$

$$\vec{\nabla}\times\vec{B}=\begin{vmatrix} i & j & k \\ \frac{\partial}{\partial x}c & \frac{\partial}{\partial y} & \frac{\partial}{\partial z} \\ b & B_0 & 0 \end{vmatrix}=-\left(\frac{\partial b}{\partial y}\right)\vec{k}$$

The curl of ohm's law yields:

$$\vec{\nabla}\times(\vec{\nabla}\times\vec{B})=\begin{vmatrix} i & j & k \\ \frac{\partial}{\partial x} & \frac{\partial}{\partial y} & \frac{\partial}{\partial z} \\ 0 & 0 & -\frac{\partial b}{\partial y} \end{vmatrix}=-\left(\frac{\partial^2\vec{b}}{\partial y^2}\right)\vec{i}$$

$$\vec{q}\times\vec{B}=\begin{vmatrix} i & j & K \\ u & v & 0 \\ b & B_0 & 0 \end{vmatrix}=(uB_0-bv)\,\vec{k}$$

$$\vec{\nabla} \times (\vec{q} \times \vec{B}) = \begin{vmatrix} i & j & k \\ \frac{\partial}{\partial x} & \frac{\partial}{\partial y} & \frac{\partial}{\partial z} \\ 0 & 0 & uB_0 - bv \end{vmatrix} = \frac{\partial}{\partial y}(uB_0 - bv)\,\vec{i}$$

Therefore, the equation of magnetic induction is:

$$\frac{\partial}{\partial y}(uB_0 - bv) + \eta_0 \frac{\partial^2 b}{\partial y^2} = 0 \tag{17}$$

2.5. The Energy Equation

Fluid properties at the solid- fluid interface have temperature equal to that of the interface. The temperature at the interface differs with temperature on the free stream layers hence occurrence of temperature variations within the fluid.

The Mathematical formulation of equation of conservation of thermal energy is based on the first law of thermohydrodynamics. This law states that the amount of heat added to a system dQ is equal to the change in internal energy dE plus the work done dW and is expressed as $dQ = dE + dW$. Since the flow is incompressible and with variable conductivity k, the energy equation is given by:

$$\rho\left[\frac{\partial h}{\partial t} + \nabla.(h\vec{v})\right] = -\frac{Dp}{Dt} + \nabla.(k\nabla T) + \phi \tag{18}$$

Taking into consideration an incompressible flow and that $dh = cpdT$, this equation reduces to:

$$\rho C_p\left[\frac{\partial T}{\partial t} + (\vec{v}.\nabla)T\right] = k\nabla^2 T + \phi \tag{19}$$

ϕ denotes the dissipation function representing the work done against viscous forces irreversibly converted into internal energy. In our case, the Brownian motion of nanoparticles and Thermophoresis effects contribute to this function such that:

$$(\vec{\mathbf{v}}\nabla T = u\frac{\partial T}{\partial x} + v\frac{\partial T}{\partial y}$$

$$\nabla^2 T = \frac{\partial^2 T}{\partial x^2} + \frac{\partial^2 T}{\partial y^2}$$

$$\Phi = \tau\left[D_B\left(\frac{\partial C \partial T}{\partial x \partial x} + \frac{\partial c \partial T}{\partial y \partial y}\right) + \frac{DT}{T\infty}\left\{\left(\frac{\partial T}{\partial x}\right)^2 + \left(\frac{\partial T}{\partial y}\right)^2\right\}\right]$$

$$\tau = \frac{(\rho_c)_p}{(\rho_c)_f} = \frac{heatcapacityofnanoparticle}{heatcapacityofthefluid}$$

$$\mathbf{u}\frac{\partial T}{\partial x} + \mathbf{v}\frac{\partial T}{\partial y} = \alpha\left(\frac{\partial^2 T}{\partial x^2} + \frac{\partial^2 T}{\partial y^2}\right) + \tau\left[D_B\left(\frac{\partial C \partial T}{\partial x \partial x} + \frac{\partial c \partial T}{\partial y \partial y}\right) + \frac{DT}{T\infty}\left\{\left(\frac{\partial T}{\partial x}\right)^2 + \left(\frac{\partial T}{\partial y}\right)^2\right\}\right] \tag{20}$$

where $\alpha = \frac{\kappa}{\rho c_p}$

2.6. The Concentration Equation

Concentration is a measure of how much of a given species dissolves in another substance per unit volume. It deals with the diffusion of nanoparticles due to temperature gradient and Brownian motion which is as a result of the vibratory energy of fluid particles which are in continuous random motion. The bombardment between nanoparticles and fluid particles constitutes the Brownian motion. This equation is derived from the principle of conservation of mass and is used when the porous medium is saturated with the fluid and obeys Darcy's law. Concentration equation is given by:

$$\mathbf{u}\frac{\partial C}{\partial x} + \mathbf{v}\frac{\partial C}{\partial y} = D\frac{\partial^2 C}{\partial y^2} \tag{21}$$

Where $\mathbf{u}$ and $\mathbf{v}$ are the components of velocity along x and y directions respectively, C is the dimensional concentration, and D is the molecular diffusivity of Nanofluid. We derive our concentration equation from the equation of mass conservation:

$$\frac{\partial C}{\partial t} + \frac{\partial q}{\partial x} = 0 \tag{22}$$

The advection-diffusion equation gives $\mathbf{q} = UC - D\frac{\partial C}{\partial x}$. Substituting $\mathbf{q}$ in the mass conservation equation, we get:

$$\frac{\partial C}{\partial t} + \frac{\partial\left(uc - D\frac{\partial C}{\partial x}\right)}{\partial x} = 0 \tag{23}$$

$$\frac{\partial C}{\partial t} + \frac{\partial UC}{\partial x} = \frac{\partial}{\partial x}\left(D\frac{\partial C}{\partial x}\right) \tag{24}$$

For a two-dimensional steady flow with Brownian motion

and Thermophoresis effects, the concentration equation becomes:

$$\mathbf{u}\frac{\partial C}{\partial x}+\mathbf{v}\frac{\partial C}{\partial y}=D_B\left(\frac{\partial^2 C}{\partial x^2}+\frac{\partial^2 C}{\partial y^2}\right)+\frac{D_T}{T_\infty}\left(\frac{\partial^2 T}{\partial x^2}+\frac{\partial^2 T}{\partial y^2}\right) \tag{25}$$

3. Method of Solution

The goal of non-dimensionalization of the partial differential equations (PDEs) is to identify the critical parameters required for flow problem analysis. It minimizes the number of model parameters governing an incompressible fluid's flow. Each parameter represents the ratio of the forces acting on the fluid flow. The forces' relative relevance for the flow is shown by their magnitude. The results gained for a boundary experiencing a certain set of conditions can be applied to another boundary that is geometrically comparable but experiencing entirely different solutions because of non-dimensional parameters. One of the most crucial tools for mathematics in the study of fluid mechanics is dimensional analysis. It makes logic to transform the conservation equations into a non-dimensional form in order to represent various transport processes that arise in fluid dynamics problems. Non-dimensionalization allows for any analysis of any system, regardless of the material properties. It also simplifies the understanding of the system's controlling flow parameters during investigation, generalizes the geometry's size and shape, and provides insight into the physical problem before an experiment is conducted.

The right scale selection helps to accomplish these goals. Therefore, non-dimensional variables are provided along with the boundary conditions in order to obtain the dimensionless form of the governing equations.

Through the use of similarity transformation, the coupled nonlinear partial differential equations governing the Casson Nanofluid past the wedge in the presence of an induced magnetic field are subsequently reduced to a coupled nonlinear ordinary differential equation.

This numerical method provides more accurate approximations and is efficient for both initial and boundary values, making it suitable for index -2 and higher Differential-Algebraic systems of Equations (DAEs). It is also adaptable and easy to apply to a range of situations.

Through the use of the MATLAB function bvp4c, a fourth-order accurate collocation-based solver provides a numerical solution of the resulting boundary value problem. The effects of relevant physical entities on the temperature, velocity, and induced magnetic fields of the nanofluid are graphically presented, while the rates of mass transfer, heat transfer, and local skin friction are tabulated.

3.1. Non-Dimensionalization

The goal of non-dimensionalization of the PDEs is to identify the critical parameters required for flow problem analysis. It minimizes the number of model parameters governing an incompressible fluid's flow. Each parameter represents the ratio of the forces acting on the fluid flow. The forces relative relevance for the flow is shown by their magnitude. The results gained for a boundary experiencing a certain set of conditions can be applied to another boundary that is geometrically comparable but experiencing entirely different solutions because of non-dimensional parameters.

One of the most crucial tools for mathematics in the study of fluid mechanics is dimensional analysis. It makes logic to transform the conservation equations into a non-dimensional form in order to represent various transport processes that arise in fluid dynamics problems.

Non-dimensionalization allows for any analysis of any system, regardless of the material properties. It also simplifies the understanding of the system's controlling flow parameters during investigation, generalizes the geometry's size and shape, and provides insight into the physical problem before an experiment is conducted.

The right scale selection helps to accomplish these goals. Therefore, non-dimensional variables are provided along with the boundary conditions in order to obtain the dimensionless form of the governing equations.

Through the use of similarity transformation, the coupled nonlinear partial differential equations governing the Casson Nanofluid past the wedge in the presence of an induced magnetic field are subsequently reduced to a coupled nonlinear ordinary differential equation. The non-dimensional parameters to be used in non-dimensionalisation include:

a. Prandl Number

The Prandtl number (*Pr*) is the ratio of fluid properties controlling the velocity and the temperature distributions. It is defined as the ratio of viscous force to thermal force.

$$Pr=\frac{\mu C_p}{\kappa_f}=\frac{\vartheta}{\alpha}$$

where

$\alpha=\frac{\kappa_f}{\rho C_p}$ is the thermal diffusivity

$$\vartheta=\frac{\mu}{\rho}$$

b. Schmidt number

The Schmidt number (*Sc*) is the measure of the relative effectiveness of momentum and mass transport by diffusion in the velocity and the concentration boundary layers.

$$Sc=\frac{\vartheta}{D}$$

c. Reynolds Number

The Reynols number (*Re*) is the measure of the ratio of inertia force to the viscous force

$$Re=\frac{xu_x}{\vartheta}$$

d. Magnetic Field Parameter

Magnetic Field Parameter(*M*) is the measure of square root of the ratio of magnetic force to the ineartia force. The PDE form of equation can be converted to ODE using similarity functions.

Stream function ψ is a scalar function used to represent the velocity components of the fluid flow in two dimensional, incompressible flow. Its partial derivatives give the velocity components of the flow.

The following dimensionless local similarity variables are considered:

$$\eta = y\left(\frac{a}{\vartheta\infty}\right)^{\frac{1}{2}}$$

$$\mathbf{u} = axf^{'}(\eta)$$

$$\mathbf{v} = -\left(a\vartheta_{\infty}\right)^{\frac{1}{2}} f(\eta)$$

$$\theta(\eta) = \frac{T - T_m}{T_\infty - T_m}$$

$$\Phi(\eta) = \frac{C - C_\infty}{C_w - C\infty}$$

$$\psi = (a\vartheta)^{1/2} xf(\eta)$$

$$\mathbf{b} = -B_0 H^{'}(\eta)$$

$$\eta = (a/\vartheta)^{1/2} y$$

3.2. Equation of Continuity

$$\mathbf{u} = \frac{\partial\psi}{\partial y}$$

$$\mathbf{v} = -\frac{\partial\psi}{\partial x}$$

$$\frac{\partial u}{\partial x} + \frac{\partial\vartheta}{\partial y} = 0$$

$$u = \frac{\partial\psi}{\partial y} = \frac{\partial\psi}{\partial\eta}.\frac{\partial\eta}{\partial y}$$

$$\frac{\partial\psi}{\partial\eta} = \frac{\partial}{\partial\eta}[(a\vartheta)^{1/2} xf(\eta)] = (a\vartheta)^{1/2} xf'(\eta)$$

$$\frac{\partial\eta}{\partial y} = \frac{\partial}{\partial y}[(a/\vartheta)^{1/2} y] = (a/\vartheta)^{1/2} = axf'(\eta)$$

$$u = \frac{\partial\psi}{\partial\eta}.\frac{\partial\eta}{\partial y} = (a\vartheta)^{1/2} xf'(\eta).(a/\vartheta)^{1/2} = axf'(\eta)$$

$$\frac{\partial u}{\partial x} = \frac{\partial}{\partial x}[axf'(\eta)] = af'(\eta)$$

$$v = -\frac{\partial\psi}{\partial x} = -(a\vartheta)^{1/2} f(\eta)$$

$$\frac{\partial v}{\partial y} = -\frac{\partial}{\partial y}[(a\vartheta)^{1/2} f(a/\vartheta)^{1/2} y] = -af'(\eta)$$

$$\frac{\partial u}{\partial x} + \frac{\partial v}{\partial y} = af'(\eta) + -af'(\eta) = 0$$

Thus the equation of continuity is satisfied.

3.3. Momentum Equation

The specific momentum equation for the flow past the wedge yielded:

$$u\frac{\partial u}{\partial x} + v\frac{\partial u}{\partial y} = U(\infty)\frac{du_\infty}{dx} + \vartheta(1 + \frac{1}{\beta})(\frac{\partial^2 u}{\partial x^2} + \frac{\partial^2 u}{\partial y^2}) - \frac{\sigma B_0^2(u - u_\infty)}{\rho} + \frac{\sigma B_0 bv}{\rho} \tag{26}$$

$$u\frac{\partial u}{\partial x} = a^2 x(f^{'})^2$$

$$v\frac{\partial u}{\partial y} = -a^2 xff^{''}$$

$$U\infty\frac{dU\infty}{dx} = a^2 x$$

$$\frac{\partial\mathbf{u}}{\partial\mathbf{x}} = af^{'}(\eta)$$

$$\frac{\partial^2 u}{\partial x^2} = 0$$

$$\frac{\partial u}{\partial y} = a^{3/2}\vartheta^{-1/2} xf^{''}(n)$$

$$\frac{\partial^2 u}{\partial y^2} = \frac{a^2}{\vartheta} f^{'''}$$

$$\frac{\sigma B_0^2 u}{\rho} = \frac{\sigma B_0^2(axf(n))}{\rho}$$

$$\frac{\sigma B_0^2 u_\infty}{\rho} = \frac{\sigma B_0^2 ax}{\rho}$$

$$\frac{\sigma B_0 bv}{\rho} = \frac{\sigma B_0^2}{\rho B_0}(-axH^{'}(\eta)) = \frac{\sigma}{\rho}\frac{B_0^2}{B_0}a^{3/2}x\vartheta^{1/2}H^{'}(\eta)f(\eta)$$

$$\frac{a^2x(f^{'})2}{a^2} - \frac{a^2xff^{''}}{a^2x} = \frac{a^2x}{a^2x} + \frac{\vartheta(1+\frac{1}{\beta})(\frac{a^2x}{\vartheta}f^{'''}}{a^2x} - \frac{\sigma B_0^2 axf^{'}(\eta)}{a^2x\rho} + \frac{\sigma B_0^2 ax}{a^2x\rho} + \frac{\sigma B_0^2 a^{3/2}x\vartheta^{1/2}H^{'}(\eta)f(\eta)}{a^2x}$$

$$(f^{'})^2 - ff^{''} = 1 + (1+\frac{1}{\beta})f^{'''} - \frac{\sigma B_0^2}{a\rho}f^{'}(n) + \frac{\sigma B_0^2}{a\rho} + \frac{\sigma B_0^2(a\vartheta)^{1/2}H^{'}(\eta)f(\eta)}{a\rho B_0}$$

$$\frac{\sigma B_0^2(a\vartheta)^{1/2}H^{'}(\eta)f(\eta)}{a\rho B_0}$$

$$\sqrt{\left(\frac{\sigma B_0(a\vartheta)^{\frac{1}{2}}}{a\rho}\right)^2}$$

$$\sqrt{\frac{\sigma B_0^2\sigma\vartheta}{a\rho^2}}$$

$$\sqrt{\frac{1}{Pm}.M}$$

$$(f^{'})^2 - ff^{''} = 1 + (1+\frac{1}{\beta})f^{'''} - M(f^{'}(\eta)-1) + M^{\frac{1}{2}}Pm^{-\frac{1}{2}}$$

$$(1+\frac{1}{\beta})f^{'''} + ff^{''} - (f^{'})^2 + 1 - M\left(f^{'}(\eta)-1\right) + M^{\frac{1}{2}}Pm^{+\frac{1}{2}}H^{'}(\eta)f(\eta) = 0 \tag{27}$$

equation 27 is the dimensionless momentum equation for the flow past the wedge.

3.4. Energy Equation

$$\mathbf{u}\frac{\partial T}{\partial x} + \mathbf{v}\frac{\partial T}{\partial y} = \frac{k}{\rho c_p}\frac{\partial^2 T}{\partial y^2} + \tau\left(D_B\frac{\partial c}{\partial y}\frac{\partial T}{\partial y} + \frac{DT}{T_\infty}\left(\frac{\partial T}{\partial y}\right)^2\right) \tag{28}$$

$$\theta(\eta) = \frac{T - T_\infty}{T_w - T_\infty}$$

$$T = (T_w - T_\infty)\theta(\eta) + T_\infty$$

$$\phi(\eta) = \frac{C - C_\infty}{C_w - C_\infty}$$

$$C = (C_w - C_\infty)\phi(\eta) + C_\infty$$

$$\frac{\partial T}{\partial x} = 0$$

$$\mathbf{u}\frac{\partial T}{\partial x} = 0$$

$$\frac{\partial T}{\partial y} = (T_w - T_\infty)\phi^{'}(\eta)(\frac{a}{v})^{\frac{1}{2}}$$

$$\mathbf{v}\frac{\partial T}{\partial y} = -(av)^{\frac{1}{2}}f(\eta)\phi^{'}(\eta)(T_w - T_\infty)(\frac{a}{v})^{\frac{1}{2}} = -a(T_w - T_\infty)f(\eta)\phi^{'}(\eta)$$

$$\frac{\partial^2 T}{\partial x^2} = 0$$

$$\frac{\partial^2 T}{\partial y^2} = \frac{\partial}{\partial y}\left(T_w - T_\infty\right)\phi^{'}(\eta)(\frac{a}{v})^{\frac{1}{2}} = \frac{a}{v}(T_w - T_\infty)\theta^{''}$$

$$\frac{\partial C}{\partial x} = 0$$

$$\frac{\partial C}{\partial y} = \frac{\partial}{\partial y}\left((C_w - C_\infty)\phi(\frac{a}{v})^{\frac{1}{2}}y + C_\infty\right) = (\frac{a}{v})^{\frac{1}{2}}(C_w - C_\infty)\phi^{'} - a(T_w - T_\infty)f(\eta)\phi^{'}(\eta)$$

$$= \alpha\left(\frac{a}{v}(T_w - T_\infty)\theta^{''}\right) + \tau\left[D_B(\frac{a}{v})^{\frac{1}{2}}(C_w - C_\infty)\phi^{'}(T_w - T_\infty)\theta^{'}(\frac{a}{v})^{\frac{1}{2}}\right] + \tau\frac{D_T}{T_\infty}\left[0 + (T_w - T_\infty)^2(\theta^{'})^2(\frac{a}{v})\right] \quad (29)$$

$$-f\theta^{'} = \theta^{''} + \frac{\tau D_B(C_w - C_\infty)}{\mathbf{v}}\theta^{'}\phi^{'} + \tau\frac{D_T}{T_\infty \mathbf{v}}(T_w - T_\infty)(\theta^{'})^2 \quad (30)$$

Brownian Parameter $N_b = \frac{D_B(C_w - C_\infty)\tau}{\mathbf{v}}$

Thermophoresis Parameter $N_t = \frac{D_T(T_w - T_\infty)\tau}{\mathbf{v}T_\infty}$

$$-f\theta^{'}Pr = \theta^{''} + PrNb\theta^{'}\phi^{'} + PrNt(\theta^{'})^2$$

$$\theta^{''} + Prf\theta^{'} + PrNb\theta^{'}\phi^{'} + PrNt(\theta^{'})^2 = 0 \quad (31)$$

Equation 31 is the dimensionless energy equation

3.5. Magnetic Induction Equation

$$\frac{\partial}{\partial y}(uB_0 - bv) + \eta_0\frac{\partial^2 b}{\partial y^2} = 0$$

$$b = -axH^{'}(\eta)$$

$$v = -(a\vartheta)^{\frac{1}{2}}f(\eta)$$

$$\eta = (\frac{a}{\vartheta})^{1/2}y, u = axf^{'}(\eta)$$

$$\frac{\partial b}{\partial y} = -axH^{''}(\frac{a}{\vartheta})^{\frac{1}{2}} = -a^{\frac{3}{2}}x\vartheta^{\frac{-1}{2}}H^{''}(\eta)$$

$$\frac{\partial^2 b}{\partial^2 y} = -a^{\frac{3}{2}}xH^{'''}(\frac{a}{\vartheta})^{\frac{1}{2}}.\vartheta^{-\frac{1}{2}} = -\frac{a^2 x}{\vartheta}H^{'''}(\eta)$$

$$v\frac{\partial b}{\partial y} = -(a\vartheta)^{\frac{1}{2}}f(\eta).- a^{\frac{3}{2}}xH^{''}(\eta).\vartheta^{\frac{1}{2}} = a^2 xf(\eta)H^{''}(\eta)$$

$$b\frac{\partial v}{\partial y} = -axH^{'}(\eta).- af^{'}(\eta) = a^2\mathbf{x}H^{'}(\eta)F^{'}(\eta)$$

$$\frac{\partial u}{\partial y} = axf^{''}(\frac{a}{\vartheta})^{\frac{1}{2}} = a^{\frac{3}{2}}xf^{''}(\eta).\vartheta^{\frac{-1}{2}}$$

$$B_0\frac{\partial u}{\partial y} = a^{\frac{3}{2}}xf^{''}(\eta)\vartheta^{\frac{-1}{2}}B_0$$

$$-\eta_0\frac{a^2 x}{\vartheta}H^{'''} = a^2 x(\eta)H^{''}(\eta) + a^2 xH^{'}(\eta)f^{'}(\eta) - B_0 a^{\frac{3}{2}}f^{''}(\eta)\vartheta^{\frac{-1}{2}} = 0$$

dividing through by $a^2 x\eta_0$ we get

$$H^{'''} + f(\eta)H^{''}(\eta)\frac{\vartheta}{\eta_0} + H^{'}(\eta)f^{'}(\eta)\frac{\vartheta}{\eta_0} - B_0(\frac{v}{a})^{\frac{1}{2}}\frac{f^{''}(\eta)}{\eta_0} = 0$$

$$B_0(\frac{\vartheta}{a})^{\frac{1}{2}}\frac{f^{''}(\eta)}{\eta_0}$$

$$\sqrt{\left(\frac{B_0}{\eta_0}\left(\frac{\vartheta}{a}\right)^{\frac{1}{2}}\right)^2}$$

$$\sqrt{\frac{B_0^2}{a\eta_0}.\frac{\vartheta}{\eta_0}} = \sqrt{M.Pm}$$

$$\frac{\vartheta}{\eta_0} = Pm$$

$$H^{'''} + Pmf(\eta)H^{''}(\eta) + PmH^{'}f'(\eta) - \sqrt{\left(\frac{B_0}{\eta_0}(\frac{\vartheta}{a})^{\frac{1}{2}}\right)^2}$$

$$H^{'''} + Pmf(\eta)H^{''}(\eta) + PmH^{'}(\eta)f^{'}(\eta) - M^{\frac{1}{2}}Pm^{\frac{1}{2}}f^{''}(\eta) = 0 \tag{32}$$

equation 32 is the dimensionless magnetic induction equation.

3.6. Concentration Equation

$$\mathbf{u}\frac{\partial C}{\partial x} + \mathbf{v}\frac{\partial C}{\partial y} = D_B\left(\frac{\partial^2 C}{\partial x^2} + \frac{\partial^2 C}{\partial y^2}\right) + \frac{D_T}{T_\infty}\left(\frac{\partial^2 T}{\partial x^2} + \frac{\partial^T}{\partial y^2}\right) \tag{33}$$

$$\mathbf{u} = axf^{'}(\eta)$$

$$\mathbf{v} = -(a\vartheta)^{\frac{1}{2}}f(\eta)$$

$$\mathbf{n} = (\frac{a}{\vartheta})^{\frac{1}{2}}y$$

$$C = (C_w - C_\infty)\phi(\eta) + C_\infty$$

$$\frac{\partial C}{\partial y} = (C_w - C_\infty)\phi^{'}(\eta)(\frac{a}{v})^{\frac{1}{2}}$$

$$\mathbf{u}\frac{\partial C}{\partial x} = 0$$

$$\mathbf{v}\frac{\partial C}{\partial y} = -(av)^{\frac{1}{2}}f(\eta).(C_w - C_\infty)\phi^{'}(\eta)(\frac{a}{v})^{\frac{1}{2}} = -a(C_w - C_\infty)\phi^{'}(\eta)f(\eta)$$

$$\frac{\partial^2 C}{\partial x^2} = 0$$

$$\frac{\partial^2 C}{\partial y^2} = \frac{\partial}{\partial y}\left((C_w - C_\infty)\phi^{'}(\eta)(\frac{a}{v})^{\frac{1}{2}}\right) = (C_w - C_\infty)\phi^{''}(\eta)(\frac{a}{v})$$

$$\frac{\partial^2 T}{\partial x^2} = 0$$

$$\frac{\partial^2 T}{\partial y^2} = (\frac{a}{v})(T_w - T_\infty)\theta^{''}(\eta)$$

$$-a(C_w - C_\infty)\phi^{'}(\eta)f(\eta) = D_B\left((\frac{a}{v})(C_w - C_\infty)\phi^{''}(\eta)\right) + \frac{D_T}{T\infty}\left[(\frac{a}{v})(T_w - T_\infty)\theta^{''}(\eta)\right]$$

$$\frac{v}{D_B}\phi^{'}(\eta)f(\eta) + \phi^{''}(\eta) + \frac{D_T}{T_\infty D_B}\frac{T_w - T_\infty}{C_w - C_\infty}\theta^{''}(\eta) = 0$$

$$\frac{v}{D_B} = Sc$$

$$Sc\phi^{'}(\eta)f(\eta) + \phi^{''}(\eta) + \frac{Nt}{Nb}\theta^{''}(\eta) = 0$$

3.7. Boundary Conditions

The following boundary conditions were employed so as to govern the behaviour of the flow at wedge boundaries to the free surface of the fluid flow past the wedge. At $y = 0$,

$$\eta = \left(\frac{a}{\vartheta}\right)^{\frac{1}{2}} y$$
$$\eta = 0$$
$$U_w = ax; U = axf^{'}\eta$$
$$f^{'} = 1$$
$$v = 0; v = -\left(a\vartheta\right)^{\frac{1}{2}} f(\eta)$$
$$f = 0; \phi = 1$$

As

$$y \to \infty$$
$$\eta \to \infty$$
$$u \to 0$$

,

$$f^{'} \to 0$$
$$T \to T_\infty, \theta \to 0$$
$$C \to C_\infty, \Phi \to 0$$

The dimensionless boundary conditions are:
At $\eta = 0$, $f^{'} = 1$,$f = 0$, $\theta^{'} = Bi\,(\theta - 1)$, $\phi = 1$
As $\eta \to \infty$,$f^{'} = 0$,$\theta \to 0$, $\phi \to 0$

4. Reduction of Order of the ODEs

$$(1 + \frac{1}{\beta})f^{'''} + ff^{''} - (f^{'})^2 + 1 - M\left(f^{'}(\eta) - 1\right) + M^{\frac{1}{2}} Pm^{-\frac{1}{2}} f(\eta)H^{'}(\eta) = 0$$
$$H^{'''} + Pmf(\eta)H^{''}(\eta) + PmH^{'}(\eta)f^{'}(\eta) - M^{\frac{1}{2}} Pm^{\frac{1}{2}} f^{''}(\eta) = 0$$
$$\theta^{''} + Prf\theta^{'} + PrNb\theta^{'}\phi^{'} + PrNt(\theta^{'})^2 = 0$$
$$Sc\phi^{'}(\eta)f(\eta) + \phi^{''}(\eta) + \frac{Nt}{Nb}\theta^{''}(\eta) = 0$$

Let:

$$y_1 = f$$
$$y_2 = f^{'}$$
$$y_3 = f^{''}$$
$$y_4 = H$$
$$y_5 = H^{'}$$
$$y_6 = H^{''}$$
$$y_7 = \theta$$
$$y_8 = \theta^{'}$$
$$y_9 = \phi$$
$$y_{10} = \phi^{'}$$

$$\dot{y_3} = \frac{\beta}{1+\beta}\left\{-y_1y_3 + y_2^2 - 1 + M\left(y_2 - 1\right) + \left(\frac{M}{Pm}\right)^{\frac{1}{2}} y_1y_5\right\}$$

$$H^{'''} = -PmfH^{''} - Pmf^{'}H^{'} - (MPm)^{\frac{1}{2}} f^{''}$$

$$\dot{y_6} = Pm\left(-y_1y_6 - y_2y_5\right) + (MPm)^{\frac{1}{2}} y_3$$

$$\theta^{''} + Pr f\theta^{'} + PrNb\theta^{'}\phi^{'} + PrNt(\theta^{'})^2 = 0$$

$$\theta^{''} = -Pr f\theta^{'} - PrNb\theta^{'}\phi^{'} - PrNt(\theta^{'})^2$$

$$\dot{y_8} = -Pry_1y_8 - PrNby_1y_{10} - PrNty_8^2$$

$$Sc\phi^{'}f + \phi^{''} + \frac{Nt}{Nb}\theta^{''} = 0$$

$$\phi^{''} = -\frac{Nt}{Nb}\theta^{''} - Scf\phi^{'}$$

$$\dot{y_{10}} = -\frac{Nt}{Nb}\dot{y_8} - Scy_1y_8$$

$$\dot{y_{10}} = -\frac{Nt}{Nb}\left(-Pry_1y_8 - PrNby_1y_{10} - PrNty_8^2\right) - Scy_1y_8$$

The system of first order transformed equations becomes:

$$\dot{y_3} = \frac{\beta}{1+\beta}\left\{-y_1y_3 + y_2^2 - 1 + M\left(y_2 - 1\right) + \left(\frac{M}{Pm}\right)^{\frac{1}{2}} y_1y_5\right\}$$

$$\dot{y_6} = Pm\left(-y_1y_6 - y_2y_5\right) - (MPm)^{\frac{1}{2}} y_3$$

$$\dot{y_8} = -Pry_1y_8 - PrNby_1y_{10} - PrNty_8^2$$

$$\dot{y_{10}} = -\frac{Nt}{Nb}\left(-Pry_1y_8 - PrNby_1y_{10} - PrNty_8^2\right) - Scy_1y_8$$

5. Numerical Simulations

Through the use of the MATLAB function bvp4c, a fourth-order accurate collocation-based solver provides a numerical solution of the resulting boundary value problem. The effects of relevant physical entities on the temperature, velocity, and induced magnetic fields of the nanofluid are graphically presented, while the rates of mass transfer, heat transfer, and local skin friction are tabulated.

5.1. Model Parameter Values

The parameters of interest in this study were assigned numerical values in order to perform an analysis of the effects on the fluid flow behaviour. The results were obtained through the implementation of the equations of fluid flow used on the MATLAB code.

Table 1. *Model Parameter Values.*

Nb	β	Nt	Prm	M	Le	Bi	Rex	(1+1/beta)f"(0)	neg_thetap(0)	neg_phip(0)
0.6	0.3	1	0.15	7	0.7	1	5	6.4705	0.6156	0.1032
1	0.3	1	0.15	7	0.7	1	5	6.3646	0.4635	0.4252
1.5	0.3	1	0.15	7	0.7	1	5	6.2788	0.3388	0.517
1	0.15	1	0.15	7	0.7	1	5	8.3138	0.4309	0.4087
1	0.6	1	0.15	7	0.7	1	5	5.0971	0.4912	0.4375
1	0.3	0.5	0.15	7	0.7	1	5	6.4427	0.576	0.5385
1	0.3	1.5	0.15	7	0.7	1	5	6.307	0.38	0.3906
1	0.3	1	0.05	7	0.7	1	5	6.3999	0.465	0.4269
1	0.3	1	0.25	7	0.7	1	5	6.3275	0.462	0.4234
1	0.3	1	0.15	3	0.7	1	5	4.7134	0.4334	0.4112
1	0.3	1	0.15	15	0.7	1	5	8.761	0.4955	0.4387
1	0.3	1	0.15	7	0.3	1	5	6.4698	0.6146	0.0299

Nb	β	Nt	Prm	M	Le	Bi	Rex	(1+1/beta)f''(0)	neg_thetap(0)	neg_phip(0)
1	0.3	1	0.15	7	2	1	5	6.2836	0.3458	1.0589
1	0.3	1	0.15	7	0.7	0.1	5	6.0697	0.2856	0.3992
1	0.3	1	0.15	7	0.7	1.3	5	6.6259	0.6425	0.4307
1	0.3	1	0.15	7	0.7	1	2.5	6.314	0.4614	0.4227
1	0.3	1	0.15	7	0.7	1	10	6.3905	0.4646	0.4265

5.2. *Effects of Parameter Variation on Velocity, Temperature, Concentration and Magnetic Induction Profiles*

5.2.1. *Nanofluid Velocity for Different Values of Casson Parameter*

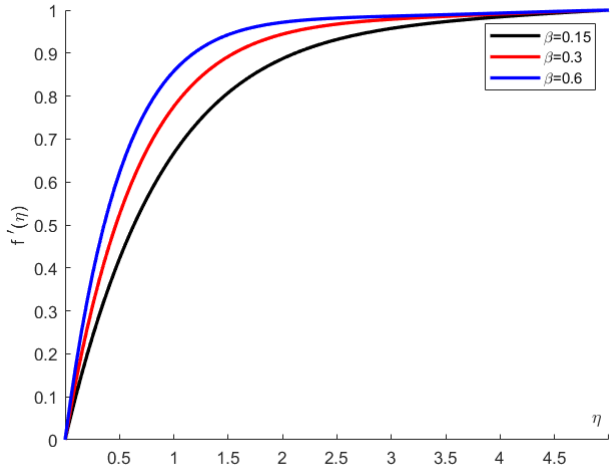

Figure 2. *Nanofluid velocity for different values of Casson parameter.*

The effect of increasing values of the Casson parameter is seen to suppress the velocity field and the thickness of boundary layer reduces. This is due to the fact that the Lorentz force has the property to slow down the motion of the conducting fluid in the boundary layer. From the momentum equation, with increment in the value of Casson Nanofluid parameter, the momentum equation tends to the momentum equation of a Newtonian fluid. Nanofluid velocity therefore increases as the effective viscous drag force decreases with the increase in Casson Nanofluid parameter. The Nanofluid velocity tends to reach the free stream velocity earlier for greater value of β.

5.2.2. *Nanofluid Velocity for Different Values of Biot Number*

The velocity profile of nanofluid flow across the wedge is notably impacted by the Biot number, which lowers the velocity distribution. Increases in the Biot number, a measurement of the proportion of conductive to convective heat transfer, are associated with this velocity drop. The greater thickness of the thermal boundary layer and the improved temperature distribution brought about by the higher Biot number are responsible for this velocity decrease.

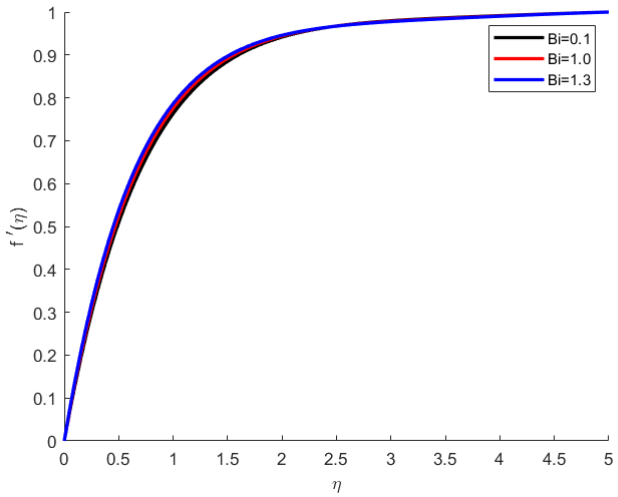

Figure 3. *Nanofluid velocity for different values of Bi.*

5.2.3. *Nanofluid Velocity for Different Values of Lewis Number*

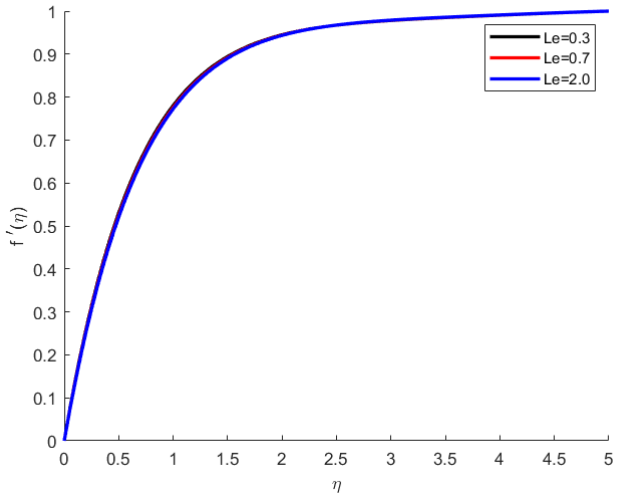

Figure 4. *Nanofluid velocity for different values of Le.*

The nanofluid's velocity is not directly impacted by the Lewis number. Heat and mass transfer are studied using the dimensionless Lewis number, which describes the ratio of mass diffusivity to thermal diffusivity. It has no direct effect on the nanofluid's velocity profile.

5.2.4. Nanofluid Velocity for Different Values of Magnetic Parameter

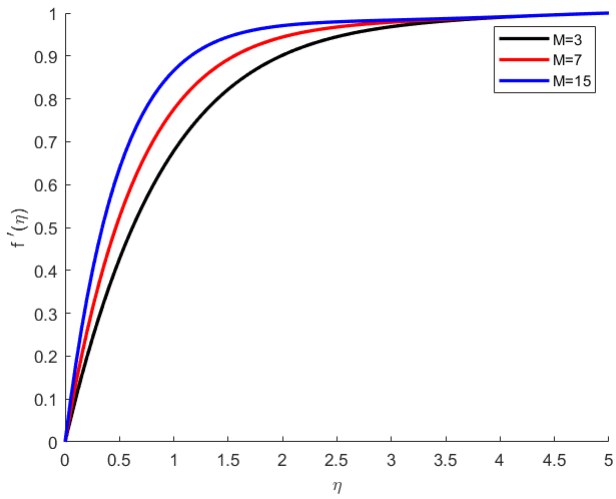

Figure 5. *Nanofluid velocity for different values of Magnetic Parameter.*

The Lorentz force exerted by the transverse magnetic field impedes the velocity field, causing the Nanofluid velocity to decrease as the magnetic parameter (M). increases.

The Lorentz force is experienced by a nanofluid flowing in a magnetic field as a result of the interaction between the charged particles (ions) in the fluid and the magnetic field. The velocity field is impeded by this force because it operates perpendicular to the direction of the fluid flow and the magnetic field.

The Lorentz force increases with increasing magnetic parameter (M), a sign of a stronger magnetic field, which results in an increased hindrance to the velocity field. As a result, whenever the magnetic parameter increases, the Nanofluid's velocity decreases.

The study of Nanofluid dynamics under magnetic fields needs to consider this phenomenon since it frequently occurs in Magneto hydrodynamic (MHD) systems.

5.2.5. Nanofluid Velocity for Different Values of Local Reynolds Number

It is here observed that the velocity profile of the Casson Nanofluid flowing past the wedge appeared to be less impacted by the local Reynolds number (Rex).

Yield stress is included in Casson fluid models, meaning that the fluid only flows when a specific stress threshold is reached.

The addition of nanoparticles can drastically change the rheological behavior when nanofluids are involved. The velocity profile is more affected by the presence of nanoparticles in the Casson fluid than by the Reynolds number.

Particle aggregation, interactions between nanoparticles and fluids, or modifications in effective viscosity brought on by nanoparticle dispersion could all be the cause of this.

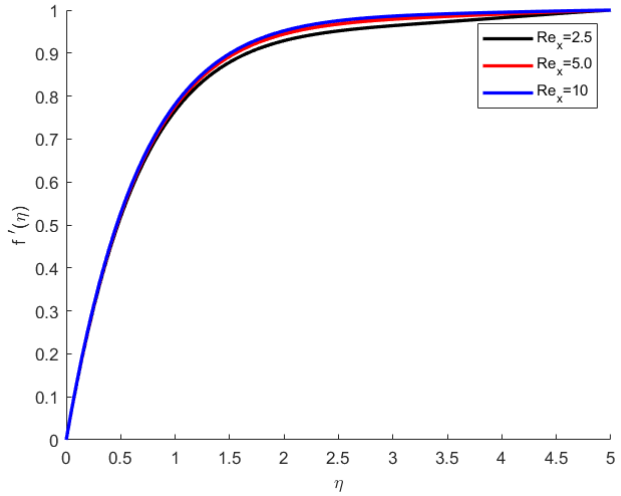

Figure 6. *Nanofluid velocity for different values of Local Reynolds Number.*

5.2.6. Nanofluid Velocity for Different Values of Magnetic Prandtl Number

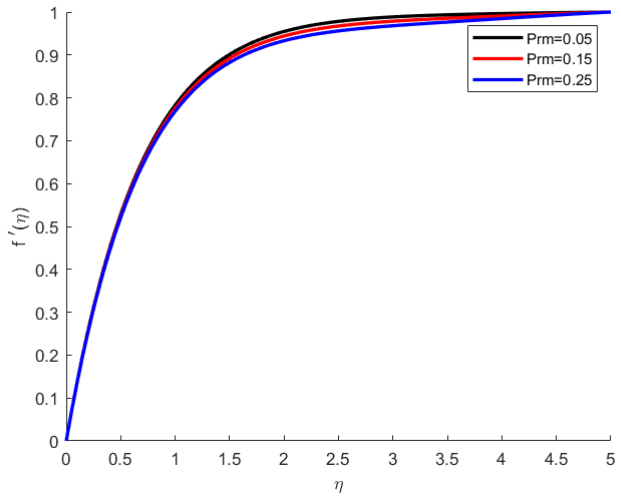

Figure 7. *Nanofluid velocity for different values of Prm.*

The Magnetic Prandtl number is a dimensionless quantity that represents the ratio of the magnetic field's effect on the fluid's momentum diffusivity to its thermal diffusivity.

For smaller Prm values, the magnetic field's influence on the fluid flow is weak compared to viscous forces. Therefore, the velocity profile of the Casson nanofluid exhibits minimal changes compared to the case without a magnetic field. As Prm increases, the magnetic field becomes more influential relative to viscous forces. This leads to alterations in the velocity profile. At higher Prm values, the magnetic forces become dominant, significantly increases the flow velocity of the Casson nanofluid.

5.2.7. Nanofluid Velocity for Different Values of Brownian Motion Parameter

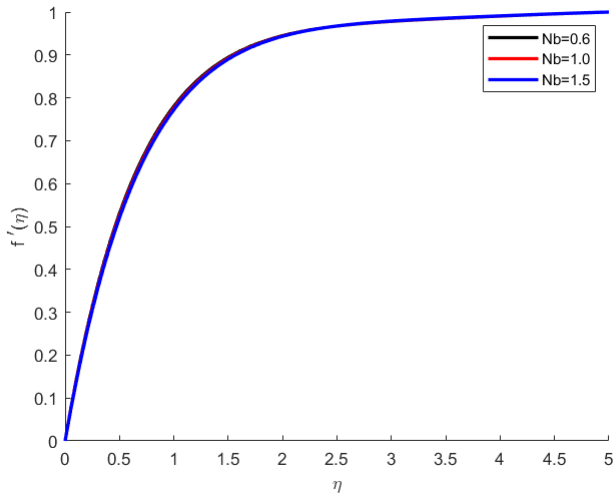

Figure 8. *Nanofluid velocity for different values of Parameter for Brownian motion.*

At low values of the Brownian motion parameter, the nanoparticles move randomly in the fluid in a limited way. As a result, Brownian motion has little effect on the velocity profile of the Casson nanofluid; instead, the velocity profile may resemble the base Casson fluid in which there are no nanoparticles, and any variations are mainly caused by the nanoparticles.

The random motion of nanoparticles intensifies with an increase in the Brownian motion parameter. The fluid's rheological characteristics may be impacted by the higher dispersion of nanoparticles brought about by this increased velocity. There are certain variations in the Casson nanofluid velocity profile compared to the basic Casson fluid case, especially in the vicinity of solid borders where Brownian motion might affect the creation of boundary layers and the aggregation of nanoparticles. High values of the Brownian motion parameter cause the nanoparticles to move randomly and disperse widely throughout the fluid. The Casson nanofluid's effective viscosity and other rheological characteristics are changed by this improved dispersion. The Casson nanofluid's velocity profile tends to differ significantly from the base Casson fluid's due to enhanced mixing and potential boundary layer changes.

5.2.8. Nanofluid Velocity for Different Values of Thermophoresis Parameter

The Thermophoresis Parameter (Nt) represents the thermophoretic motion of nanoparticles in a fluid.

The thermophoretic motion of nanoparticles is comparatively poor when the thermophoresis parameter is low. As a result, thermophoresis has little effect on the Casson nanofluid's velocity profile.

The Casson fluid's rheological characteristics and flow conditions may be the main determinants of the velocity profile; any variations may be attributed to the presence of nanoparticles rather than thermophoresis.

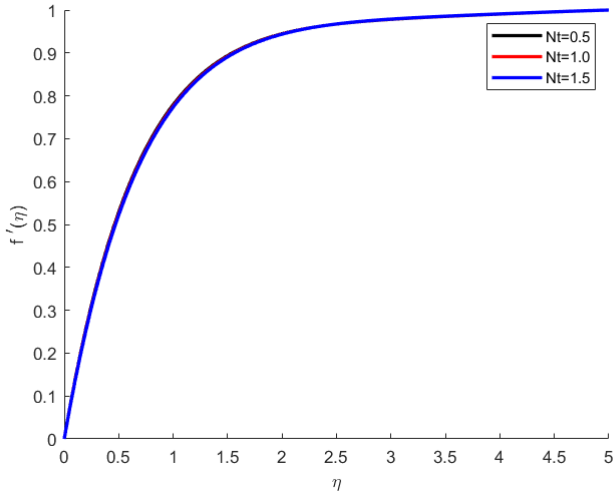

Figure 9. *Nanofluid velocity for different values of Thermophoresis Parameter.*

The thermophoretic mobility of nanoparticles in response to temperature gradients intensifies as the thermophoresis parameter rises. The fluid's effective viscosity and other rheological characteristics may be impacted by the non-uniform distribution of nanoparticles brought on by this increased thermophoretic mobility. There is a possibility that the velocity profile of the Casson nanofluid will differ from that of the base Casson fluid, especially in areas where thermophoresis effects are strong and there are large temperature gradients.

At higher values of the thermophoresis parameter, the thermophoretic motion of nanoparticles is strong, leading to significant non-equilibrium distribution of nanoparticles in the fluid. This non-equilibrium distribution can cause substantial changes in the effective viscosity and thermal conductivity of the Casson nanofluid. The velocity profile of the Casson nanofluid may deviate substantially from that of the base Casson fluid, with pronounced effects in regions with strong temperature gradients.

5.2.9. Nanofluid Temperature for Different Values of Casson Parameter

The Casson parameter significantly influences the flow of the non-Newtonian fluid.

Increasing the Casson parameter values results in an anti-symmetrical temperature distribution near the walls of the wedge.

The fluid's velocity profile, as shown by the Casson parameter, has an impact on the convective heat transfer coefficient. The rate of heat transfer within a fluid and between a fluid and its surroundings can be changed by variations in flow velocity.

Fluid rheological characteristics like viscosity are also influenced by the Casson parameter. Viscosity changes may have an impact on the fluid's ability to conduct heat. The

modifications in flow dynamics and convective heat transfer, however, might overshadow these impacts.

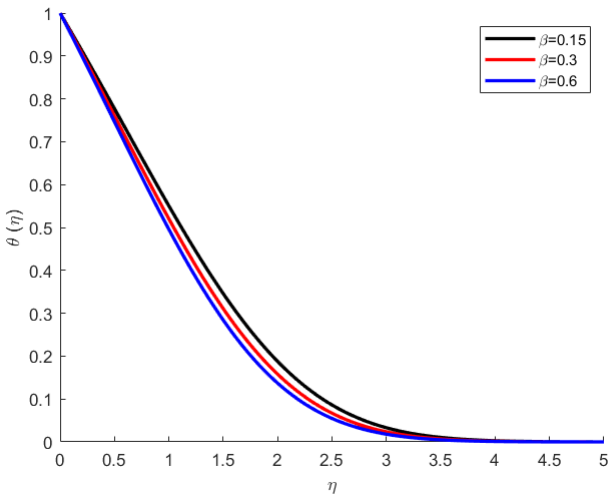

Figure 10. *Nanofluid temperature for different values of Casson Parameter.*

In Casson nanofluids, the dispersion and aggregation of nanoparticles within the fluid may be indirectly influenced by the Casson parameter. The effective thermal conductivity and heat transfer characteristics of the nanofluid can be impacted by modifications in the distribution of nanoparticles.

Although the Casson parameter directly affects the flow behaviour of Casson nanofluids, it largely has an indirect effect on the fluid's temperature through its impacts on rheological properties, flow characteristics, and convective heat transfer. It's critical to comprehend these indirect effects in order to maximise heat transfer efficiency in Casson nanofluid applications.

5.2.10. Nanofluid Temperature for Different Values of Biot Number

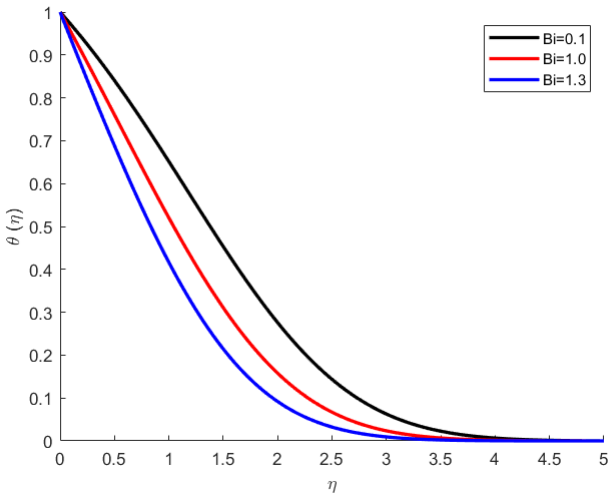

Figure 11. *Nanofluid Temperature for different values of Bi.*

The Biot number is defined as the ratio of the thermal resistance inside the solid (conduction) to the thermal resistance at the fluid-solid interface (convection).

The Biot number has a significant effect on the temperature of the nanofluid. The temperature distribution is enhanced and the thickness of the boundary layer rises as the Biot number increases.

The results reveal that higher Biot numbers result in increased temperature profiles.

5.2.11. Nanofluid Temperature for Different Values of Magnetic Parameter

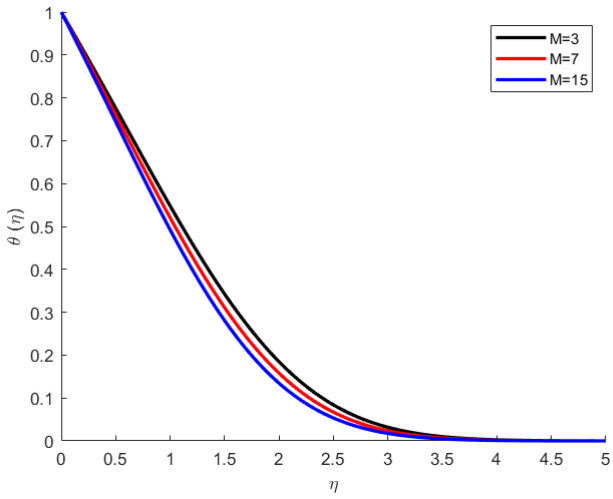

Figure 12. *Nanofluid Temperature for different values of Magnetic Parameter.*

Increasing the magnetic parameter enhances the temperature profile of nanofluids. This is caused by the transverse magnetic field's opposing Lorentz force, that works against both the fluid's flow direction and the magnetic field. This force has the ability to create turbulence and fluid motion, which improves heat transmission.

The disruption of the thermal boundary layer caused by the motion of fluid particles by the Lorentz force allows for increased heat transfer between the fluid and its surroundings. Furthermore, the Lorentz force-induced motion can enhance the fluid's nanoparticle mixing, which enhances thermal conductivity further.

Its therefore found that the temperature profile of nanofluids can be greatly improved by the opposing Lorentz force produced by the transverse magnetic field, which could make them advantageous in various heat transfer applications.

5.2.12. Nanofluid Temperature for Different Values of Lewis Number

The mass diffusivity of a fluid and its thermal diffusivity are related by the dimensionless Lewis number; which is the ratio of the thermal diffusivity to the mass diffusivity. The Prandtl number(Pr) and the Schmidt number (Sc) are used to express the Lewis number. $Le = \frac{Sc}{pr}$

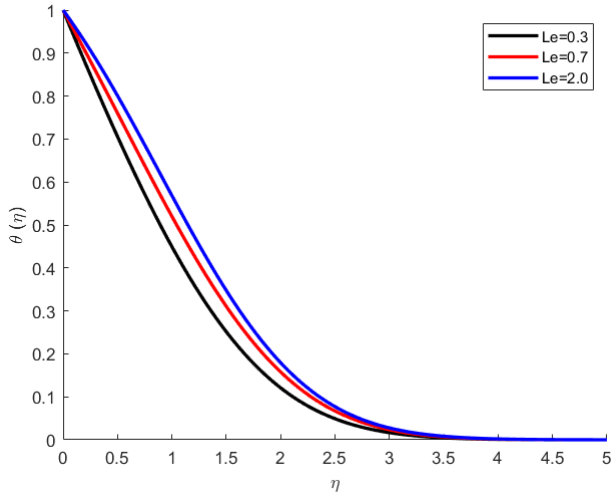

Figure 13. *Nanofluid temperature for different values of Le.*

The Schmidt number depends on both temperature and pressure, while the Prandtl number is dependent on temperature alone. Consequently, via these intermediary parameters, the Lewis number is indirectly related to both temperature and pressure.

Increased diffusion of heat relative to mass diffusion is indicated by a greater Lewis number, and vice versa.

For wedge flow, which is a type of boundary layer flow, the temperature distribution along the surface of the wedge is affected by the thermal properties of the nanofluid. A higher Lewis number typically results in a thinner thermal boundary layer near the wedge surface, indicating faster thermal diffusion.

The overall thermal conductivity and heat transfer properties of the nanofluid are influenced by the Lewis number, which also has an impact on how the nanoparticles spread and diffuse within the fluid.

Lewis numbers are taken into account by researchers and engineers when examining heat transfer in wedge flow situations involving nanofluids. Depending on the required thickness of the thermal boundary layer and the rate of temperature change along the wedge surface, modifying the composition of the nanofluid or its thermal characteristics may be able to optimize heat transfer efficiency.

5.2.13. Nanofluid Temperature for Different Values of Local Reynolds Number

The wedge's surface temperature gradually rises to the free stream temperature, as seen by the temperature distribution.

The thermal boundary layer close to the wedge's surface thickens with increasing Reynolds numbers. More mixing and heat transfer within the fluid are encouraged by eddies, which results in a more even temperature distribution over the wedge's surface. When compared to laminar flow, the temperature gradients near the surface are less noticeable because turbulent mixing transfers heat through the fluid more quickly.

This research looked into laminar flow of Casson nanofluid past a wedge.

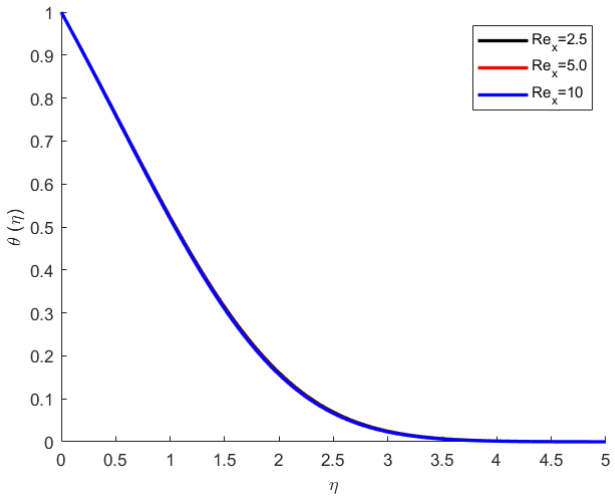

Figure 14. *Nanofluid temperature for different values of Local Reynolds Number.*

5.2.14. Nanofluid Temperature for Different Values of Magnetic Prandtl Number

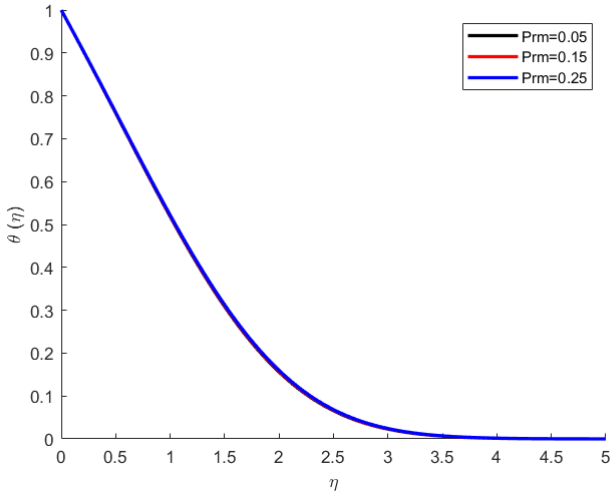

Figure 15. *Nanofluid temperature for different values of Prm.*

The ratio of thermal diffusivity to magnetic diffusivity in magnetohydrodynamics (MHD) is expressed by the dimensionless Magnetic Prandtl number.

When the magnetic Prandtl numbers are relatively low, the magnetic diffusivity is much lower than thermal diffusivity, temperature gradients are influenced more by thermal diffusivity than by magnetic effects. LowerPr_m values imply that thermal effects dominate. Therefore, there is no significant impact of the Magnetic Prandtl number on the temperature of the Casson nanofluid flowing past the wedge.

5.2.15. Nanofluid Temperature for Different Values of Brownian Motion Parameter

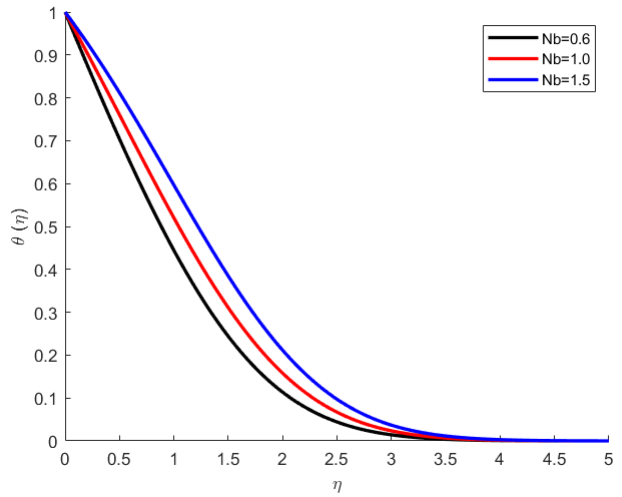

Figure 16. Nanofluid temperature for different values of Parameter for Brownian motion.

The Brownian motion parameter has an impact on the temperature distribution of the nanofluid.

It is evident that the temperature distribution increased with increasing Brownian motion parameter.

The thermal boundary layer close to the wedge surface tends to be thinner because of increased Brownian motion and higher thermal conductivity of nanofluids. This is due to the fact that heat moves from the solid surface into the fluid more effectively, which lowers the temperature differential close to the surface.

5.2.16. Nanofluid Temperature for Different Values of Thermophoresis Parameter

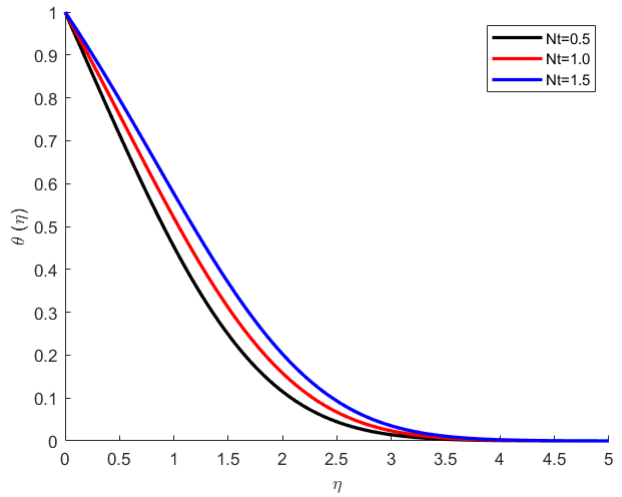

Figure 17. Nanofluid temperature for different values of Thermophoresis Parameter.

The thermophoresis parameter has an affect on the distribution of heat in the nanofluid. As the thermophoresis parameter is increased, the temperature distribution is greater.

Its demonstrated that greater thermophoresis parameter values result in higher temperature values all through the regime. A non-uniform distribution of nanoparticles is the result of the nanoparticles moving in a different direction of the temperature gradient due to the thermophoretic forces generated by greater Nt values. This uneven dispersion raises the nanofluid's temperature.

5.2.17. Nanofluid Concentration for Different Values of Casson Parameter

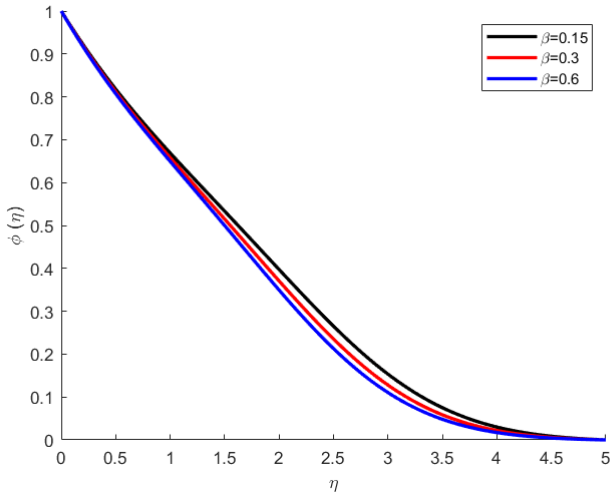

Figure 18. Nanofluid Concentration for different values of Casson Parameter.

The rheological characteristics of the nanofluid change as the concentration of nanoparticles in the base fluid rises. The yield stress and the dynamic viscosity of the nanofluid can be influenced by the presence of nanoparticles, which also affects the Casson parameter.

The Nanofluid flow was easier and behaved more like Newtonian fluids at lower Casson parameters; showing lower yield stress or more fluidity. Higher yield stress is indicated by larger Casson parameters, which means that a higher shear stress is needed to start the flow in the nanofluid.

5.2.18. Nanofluid Concentration for Different Values of Biot Number

As observed in this study, increase in the Biot number improves the concentration field, This enhancement is attributed to the increased convective heat exchange at the wedge surface, leading to a thicker thermal boundary layer.

Its therefore of great importance that in understanding Biot number effects in convective heat transfer and boundary layer dynamics.

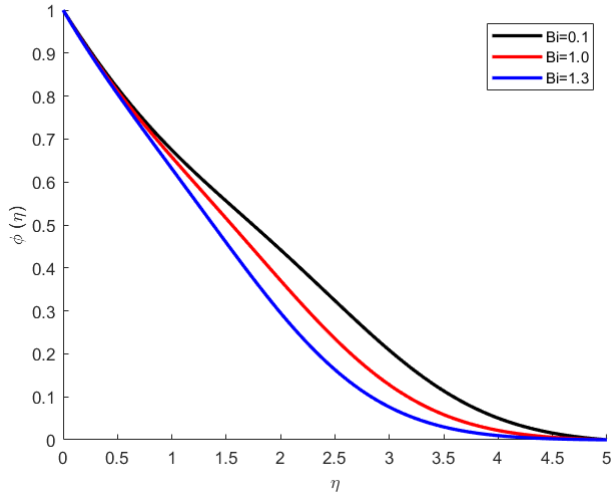

Figure 19. *Nanofluid Concentration for different values of Bi.*

5.3. Nanofluid Concentration for Different Values of Magnetic Parameter

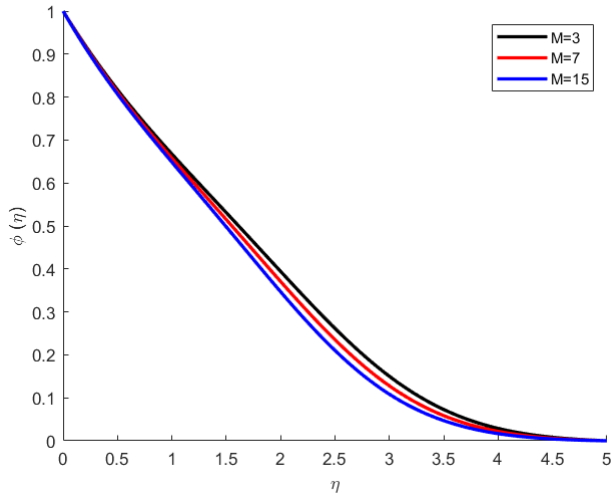

Figure 20. *Nanofluid Concentration for different values of Magnetic Parameter.*

This study demonstrates that when the magnetic field intensity or magnetic parameter increases, the concentration of nanoparticles also increases. This is due to the fact that the nanoparticles in the nanofluid move and orient more freely in the magnetic field. The orientation and velocity of the nanoparticles in the nanofluid are influenced by the magnetic field. A larger concentration of nanoparticles is the outcome of increased inter molecular collisions and the kinetic energy of the nanoparticles. This has a major effect on the nanofluid's heat transmission and fluid flow properties.

5.3.1. Nanofluid Concentration for Different Values of Lewis Number

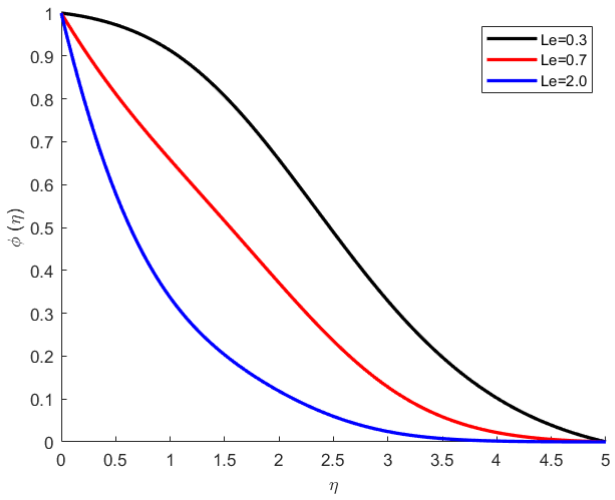

Figure 21. *Nanofluid Concentration for different values of Le.*

The concentration profiles dropped with the rise in Lewis number. This is because the mass transfer rate of nanofluid increased as the Lewis number increased resulting to a fall in nanoparticle volume fraction.

5.3.2. Nanofluid Concentration for Different Values of Local Reynolds Number

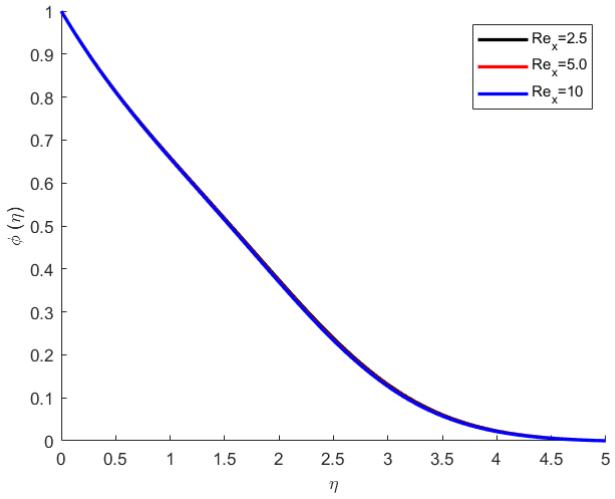

Figure 22. *Nanofluid Concentration for different values of Local Reynolds Number.*

Concentration profiles are seen to decrease as local Reynolds number increases. This is due to the fact that when the local Reynolds number rises, the mass transfer rate of the nanofluid also rises, which causes the nanoparticle volume fraction to decrease.

5.3.3. Nanofluid Concentration for Different Values of Magnetic Prandtl Number

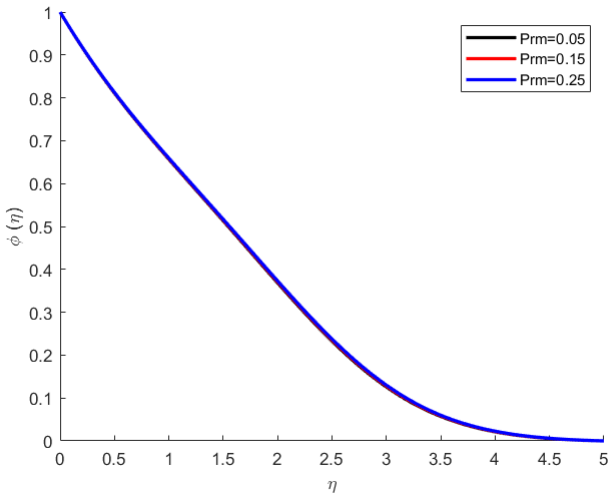

Figure 23. Nanofluid Concentration for different values of Prm.

Lower Magnetic Prandtl values indicate that, in comparison to kinematic viscosity, magnetic diffusivity is comparatively high. These circumstances result in a deeper penetration of the magnetic field into the fluid, which may strengthen the interaction between the magnetic field and the suspended nanoparticles, influencing the concentration and dispersion of nanoparticles in the nanofluid. In contrast, a larger Pr_m indicates that magnetic diffusivity is of lesser significance than the fluid's viscosity. Here, the magnetic field affects the nanoparticles less strongly and with a shallower penetration depth.

5.3.4. Nanofluid Concentration for Different Values of Brownian Motion Parameter

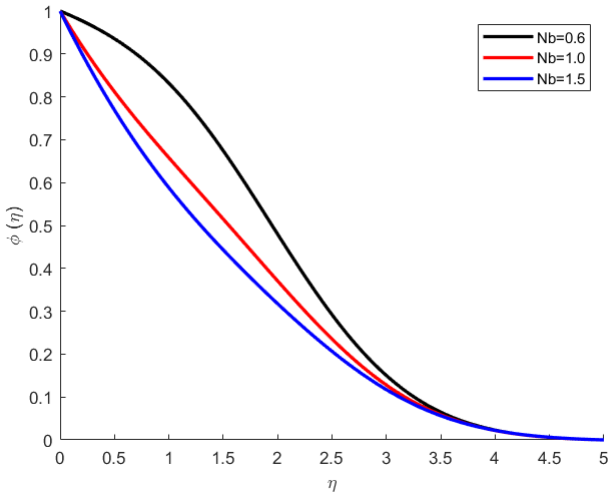

Figure 24. Nanofluid Concentration for different values of Parameter for Brownian motion.

The dimensionless Brownian motion parameter describes how strong Brownian motion is in comparison to convective motion in the fluid.

When compared to convective motion, Brownian motion is comparatively weak when the Brownian Motion Parameter is low. In such situations, nanoparticles may be less likely to assemble as a result of Brownian collisions and have a tendency to follow the fluid flow more closely. This could lead to a more uniform concentration distribution of nanoparticles in the nanofluid.

When compared to convective motion, Brownian motion is more significant with higher values of the Brownian Motion Parameter. Stronger random temperature fluctuations in this environment cause the effects of Brownian motion to be more noticeable in nanoparticles. This results in a more scattered concentration profile within the nanofluid by causing the nanoparticles to diffuse more broadly and possibly agglomerate less.

Understanding how the Brownian Motion Parameter affects nanofluid concentration is crucial for practical applications like improving heat transfer or magnetic fluid dynamics. It helps with system design when nanoparticles are utilized to alter fluid characteristics or to attain particular rheological or thermal qualities.

5.3.5. Nanofluid Concentration for Different Values of Thermophoresis Parameter

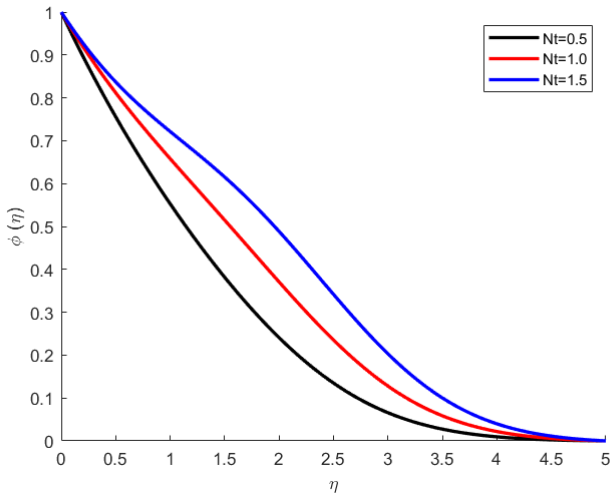

Figure 25. Nanofluid Concentration for different values of Thermophoresis Parameter.

As the Thermophoresis parameter increases, the concentration profiles decrease. This is due to the fact that when the Thermophoresis parameter increases, the mass transfer rate of the nanofluid also increases, resulting in a decrease in the volume fraction of nanoparticles.

Increasing Thermophoresis values result in the deposition or accumulation of particles preferentially in areas with temperature gradients. Consequently, gradients in the concentration profile of the nanoparticles inside the nanofluid

rise from Thermophoretic processes.

Understanding how temperature gradients impact the concentration of nanoparticles in nanofluids requires an understanding of the Thermophoresis parameter. Its impact on particle movement and deposition in the presence of temperature gradients impacts the behaviour and overall performance of nanofluids.

5.3.6. Magnetic Induction Profile for Various Values of Casson Parameter

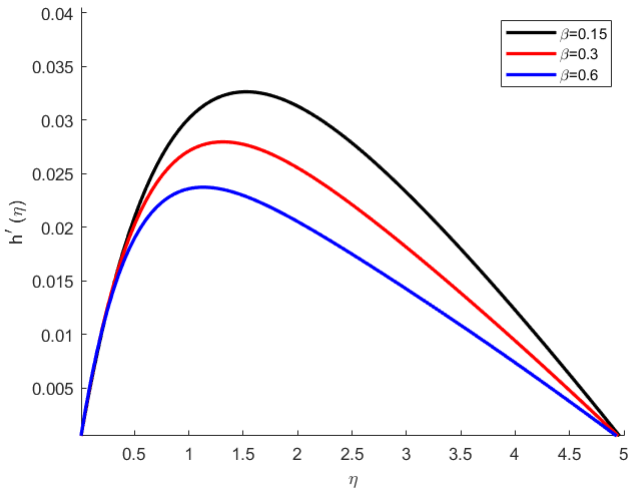

Figure 26. *Magnetic induction profile for various values of Casson Parameter.*

According to this study's observations, the magnetic induction profile rises as the Casson parameter rises. This is because the fluid's viscosity is influenced by the Casson parameter, which results in a thicker thermal boundary layer and increased magnetic induction.

In general, a greater Casson value denotes a larger yield stress and, consequently, a higher fluid viscosity. The area close to a solid surface where heat transmission mostly happens by conduction rather than convection is known as the thermal boundary layer. The fluid's viscosity determines the thickness of this boundary layer; fluids with greater viscosity generally have thicker boundary layers.

Magnetic induction occurs when an electrically conductivity fluid is exposed to a magnetic field. This happens because electromagnetic forces cause currents in the fluid to flow. Many parameters, such as the fluid's velocity and conductivity, affect the strength of the generated magnetic field, or magnetic induction. The fluid becomes more viscous when the Casson parameter is higher. In the vicinity of the solid borders, the increased viscosity causes a thicker thermal boundary layer. In turn, a thicker thermal boundary layer influences the properties of heat transfer and fluid flow, which can have an impact on the magnetic induction's pattern and intensity of induced currents. In fluid systems subjected to magnetic influence, larger Casson parameters are therefore often correlated with increased magnetic induction.

5.3.7. Magnetic Induction Profile for Various Values of Biot Number

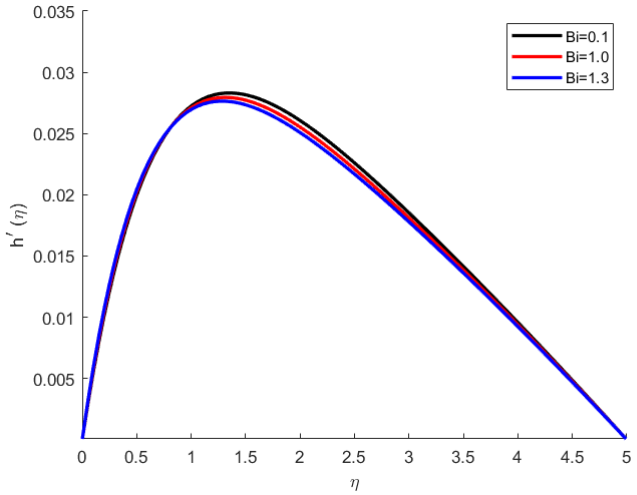

Figure 27. *Magnetic induction profile for various values of Bi.*

As observed in this study, the magnetic induction profile increases with the rise in Biot number. The Biot number represents the ratio of convective heat transfer to conductive heat transfer and an increase in Biot number enhances the convective heat transfer, thus Biot number affects the heat transfer rate, which in turn influences the magnetic induction profile.

when analyzing the magnetic induction profile and heat transfer behaviour of nanofluids, the Biot number is an essential parameter to consider.

5.3.8. Magnetic Induction Profile for Various Values of Lewis Number

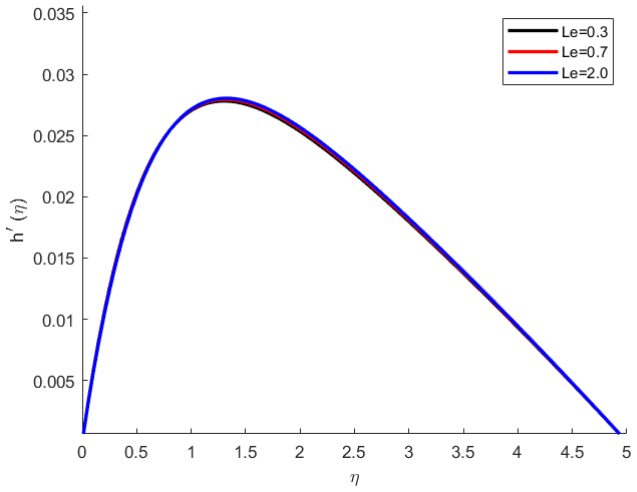

Figure 28. *Magnetic induction profile for various values of Le.*

The Lewis number (Le) is defined as the ratio of thermal diffusivity to mass diffusivity. The Lewis number affects the fluid's heat and mass transport process and further modifies the induction profile when a magnetic field is present. For Low Lewis Numbers (Le $<$ 1), mass diffusivity takes dominance over thermal diffusivity. The magnetic field usually has a greater effect on mass transport than heat transmission. The different magnetic induction patterns that arise from this have an effect on the stability and structure of the induced currents in the fluid.

Higher Lewis numbers result in greater induced magnetic fields, which enhance the fluid's interaction with the magnetic field.

5.3.9. Magnetic Induction Profile for Various Values of Local Reynolds Number

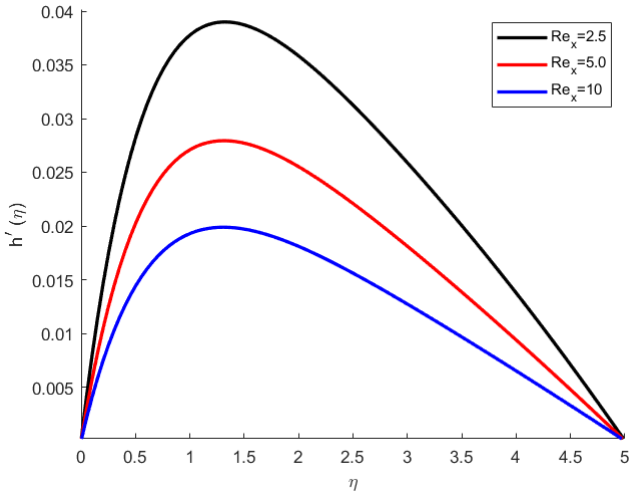

Figure 29. *Magnetic induction profile for various values of Local Reynolds Number.*

The magnetic induction profile is reduced at higher local Reynolds numbers. A decrease in magnetic force brought about by an increase in the local Reynolds number affects the magnetic induction profile. Magnetic induction profiles in an MHD system can become more dynamic and diverse with a rise in the local Reynolds number. These alterations are frequently investigated in order to comprehend the behaviour, stability, and effectiveness of MHD systems, such as those employed in electromagnetic propulsion or plasma confinement (such as fusion reactors).

5.3.10. Magnetic Induction Profile for Various Values of Magnetic Parameter

In the magnetic flux, diffusion prevails over advection for Low Magnetic Reynolds Numbers (Rm ¡ 1). In the vicinity of the conductive boundaries, the induced magnetic field is typically weak and localized. With little distortion or amplification, the magnetic induction profile exhibits a straightforward and linear relationship with the external magnetic field. When the Magnetic Reynolds Number $(1 < Rm < 10)$ is moderate, the importance of advection over diffusion grows with Rm. More intricate patterns begin to appear in the magnetic field that the fluid flow generates. The induction profile exhibits magnetic field distortion and amplification, with larger effects in areas of increased turbulence and flow velocity.

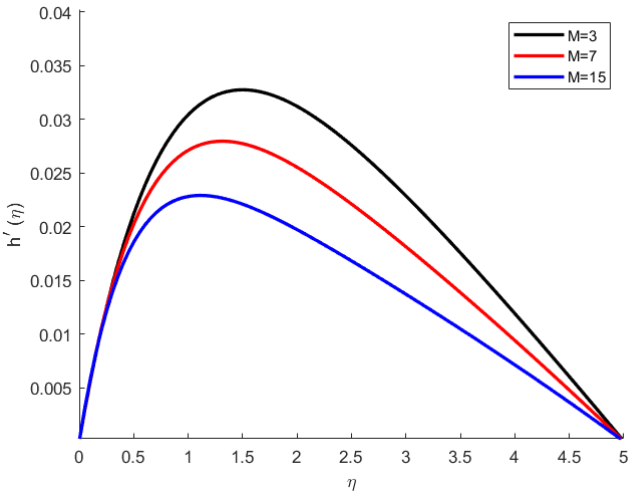

Figure 30. *Magnetic induction profile for various values of Magnetic Parameter.*

Advection prevails over diffusion in the magnetic flux at larger Magnetic Reynolds Numbers (Rm ¿ 10). There is a significant increase in the induced magnetic field, which may even become turbulent. A more complicated magnetic induction profile results from the increased prominence of magnetic structures including current sheets, eddies, and vortices. The induction profile reveals complex and strong magnetic fields dispersed across the fluid. Therefore, in MHD systems, the magnetic induction profile is highly dependent on the magnetic parameter (M). For applications in magnetic confinement fusion, plasma physics, astrophysical flows, and other domains where MHD is essential to the dynamics of magnetized fluids, understanding these variations is fundamental.

5.3.11. Magnetic Induction Profile for Various Values of Magnetic Prandtl Number

The magnetic Prandtl number (Pr_m) in MHD Casson nanofluid flow is seen to have a substantial impact on the magnetic induction profile. Low Pr_m shows that viscosity, or momentum diffusivity, predominates over magnetic diffusivity. In these situations, magnetic effects are less pronounced than viscous ones. The induced magnetic field is weaker and less noticeable. Compared to viscous forces, magnetic forces have less of an impact on the magnetic induction profile, which displays smoother and simpler patterns. When Pr_m increases, the magnetic diffusivity becomes more significant in relation to viscosity, producing stronger magnetic effects that impact fluid dynamics. As the induced magnetic field intensifies, it displays intricate spatial patterns.

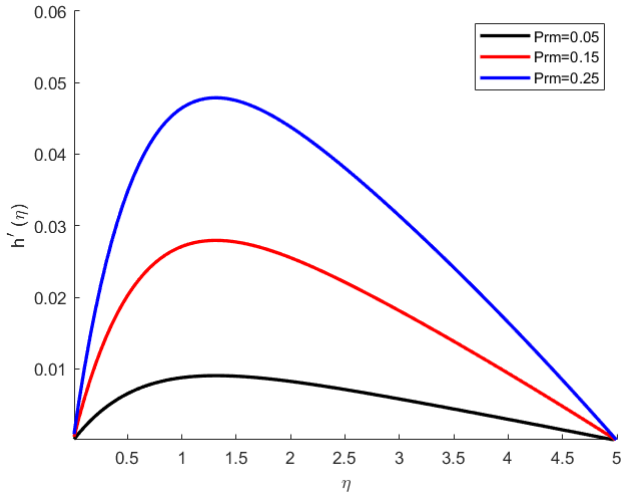

Figure 31. *Magnetic induction profile for various values of* Pr_m.

Magnetic forces are more significant in forming currents and shaping the fluid's motion. Magnetic field lines in the magnetic induction profile are amplified and concentrated in the fluid flow-influenced regions. The inclusion of nanoparticles modifies the magnetic induction profile with respect to conventional fluids and affects the strength and local distribution of the generated magnetic field.

It is essential to understand the magnetic Prandtl number in order to forecast and manage magneto hydrodynamic occurrences in Casson nanofluid flows. When analysing MHD systems' stability, efficiency, and behaviour, engineers and researchers need to take into account changes in Pr_m, especially in applications where heat transfer enhancement is involved.

5.3.12. *Magnetic Induction Profile for Various Values of Brownian Motion Parameter*

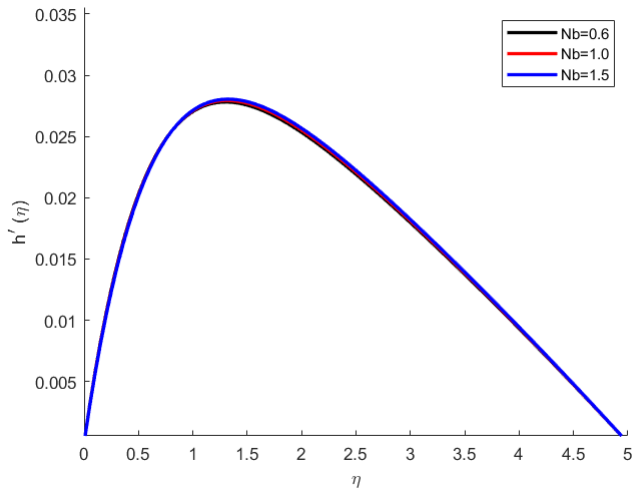

Figure 32. *Magnetic induction profile for various values of Parameter for Brownian motion.*

A decrease in the magnetic induction profile at higher Nb values is observed suggesting a weaker interaction between the fluid and the magnetic field. For lower values of the Brownian motion parameter, there is minimal impact from nanoparticles, the magnetic induction profile exhibits a smoother, more consistent behaviour that is more like to conventional MHD flow patterns.

5.3.13. *Magnetic Induction Profile for Various Values of Thermophoresis Parameter*

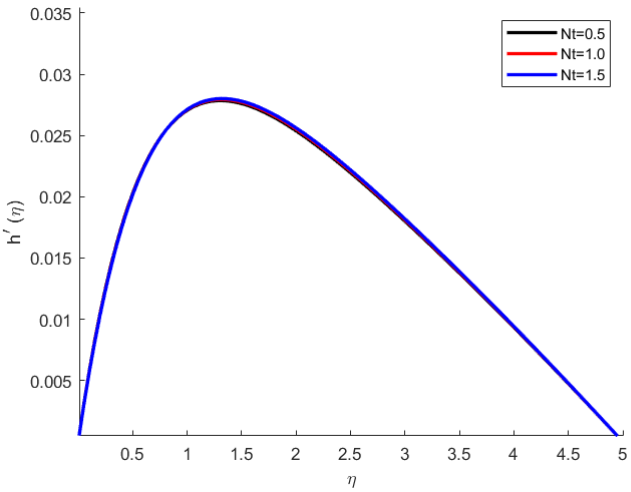

Figure 33. *Magnetic induction profile for various values of Thermophoresis Parameter.*

The magnetic induction profile decreases with higher values of Nt, suggesting a less interaction between the fluid and the magnetic field. Thermophoretic effects are weak relative to thermal diffusion for relatively lower thermophoretic effects. Because of thermophoresis, nanoparticles often closely track the temperature distribution with minimal or no migration. Both magnetic and thermophoretic forces impact the concentration and dispersion of nanoparticles in Casson nanofluid flows past a wedge, which in turn affects the magnetic induction profile. The magnetic induction profile is changed by the interaction between magnetic fields and the electric currents caused by fluid motion and the presence of nanoparticles. Thermophoresis has the ability to modify the effective magnetic properties of the nanofluid locally by causing localized increases or decreases in the concentration of nanoparticles.

5.4. *Effects of Variation of Parameters on Skin Friction, Nusselt Number and Sherwood Number on the Casson Nanofluid*

The local skin friction coefficient, local Nusselt and Sherwood numbers represent the wall shear stress, heat transfer rate, and mass transfer rate, respectively. As observed in table 1 above:

The local Skin Friction increases with increase in Magnetic parameter, Biot number and Local Reynolds number while it

reduces with increase in Thermophoresis, Casson, Brownian, Magnetic Prandtl and Lewis number Parameter.

Nusselt number increases with increase in the Casson parameter, magnetic parameter, Biot number and local Reynolds number. It however reduces with increase in Brownian Motion parameter, Thermophoresis Parameter, Magnetic Prandtl parameter and Lewis number.

The Sherwood number tend to increase with increase in Brownian Parameter, Casson parameter, Magnetic Parameter, Lewis number, Biot number and Local Reynolds number. On contrary, it reduces with rise in Thermophoresis Parameter and Magnetic Prandtl number. Magnetic Parameter represents the ratio of electromagnetic forces to viscous forces in the fluid flow. With increasing magnetic parameter values, it is found that the skin friction coefficient increases. When considering the fluid properties and flow velocity, a greater Magnetic Parameter signifies a stronger magnetic field. The velocity profile of the fluid is generally affected by the strength of the magnetic field present. When a fluid flows perpendicular to the flow direction and the magnetic field, the Lorentz force operates to reduce the fluid's velocity in MHD. In general, there is an increase in skin friction coefficient. The increased velocity gradient at the boundary layer results from the larger magnetic field's modification of the velocity profile close to the surface. Because of this modified velocity profile, the skin friction coefficient is precisely proportional to the shear stress at the surface.

6. Conclusion

When nanoparticles are added to the problem's base fluid, the flow pattern is drastically changed. The hydromagnetic field gets stronger, which amplifies the induced magnetic field and temperature distributions. This can be attributed to the distinct characteristics of the nanoparticles, which engage in magnetic field interaction to impact fluid.

The previously described data analysis validates that the subsequent outcome is attained when the magnetic Prandtl's number fluctuates, and the previously mentioned parameters are maintained constant as recommended. While the momentum boundary layer thickens with increasing magnetic induction, the energy boundary layer thickens with the development of the induced magnetic field. With magnetic induction, the concentration of nanoparticles rose.

The magnetic Prandtl number (Pr_m)in MHD Casson nanofluid flows determines the significance of viscosity versus magnetic diffusivity in structuring the induced magnetic field and its spatial distribution within the fluid, which has a substantial impact on the magnetic induction profile.

In order to allow for rising values of the Biot number and Thermophoresis parameter, the concentration and temperature fields have expanded. This indicates that the high distribution of nanoparticles is caused mostly by Thermophoresis, a technique in which particles migrate in response to a temperature gradient. The Thermophoresis parameter and Biot number are important factors to take into account when evaluating the degree of Thermophoresis and how it impacts the distribution of nanoparticles. The energy boundary layer thickens with the development of the induced magnetic field, while the momentum boundary layer thickens with increasing magnetic induction. The concentration of the nanoparticles increased with magnetic induction. The rate of heat transfer is increased when the induced magnetic field parameter increases. The problem's base fluid's flow pattern is significantly altered when nanoparticles are added. The temperature distributions and induced magnetic field are amplified as a result of the hydromagnetic field becoming stronger. This is explained by the unique properties of the nanoparticles, which interact with fluid through magnetic field interaction. It is evident that when the induced magnetic field is taken into account, shielding the internal walls of channels and nozzles is essential to preventing a hot conducting fluid from getting into contact with those walls. This is especially significant when it comes to magnetic nozzles, which are used in space propulsion to accelerate and direct a plasma jet into vacuum. The applied magnetic field in a magnetic nozzle is essential for controlling the plasma jet. The plasma experiences electric currents from the magnetic field, which provide an opposing force that pulls the plasma downstream.

An understanding of how the thermophoresis parameter affects the Casson nanofluid flow behavior is crucial for heat-transfer applications such energy conversion devices based on nanofluids, thermal insulation, and cooling systems. Quantifying these effects and directing the design and development of nanofluid-based systems for heat transfer applications can be accomplished with the use of computational simulations and experimental research.

ORCID

0000-0002-6354-8706 (Ochwach Jimrise)
0009-0000-2840-8364 (Okongo Mark)

Acknowledgments

We thank the administrative staff of the Department of Physical Sciences of Chuka University for their hospitality and assistance with matters related to our research work.

Author Contributions

Nyaga Danson: Conceptualization, Data curation, Formal Analysis, Funding acquisition, Investigation, Methodology, Project administration, Resources, Validation, Visualization

Ochwach Jimrise: Data curation, Formal Analysis, Funding acquisition, Investigation, Methodology, Project administration, Software, Validation, Visualization

Kirimi Jacob: Conceptualization, Project administration, Resources, Supervision, Validation

Okongo Mark: Supervision

Conflict of Interest

The authors declare that there are no conflict of interest with respect to the publication of this article.

References

[1] Abd El-Aziz, M. and Afify, A. A. (2018). Influences of slip velocity and induced magnetic field on mhd stagnation-point flow and heat transfer of casson fluid overa stretching sheet. Mathematical Problems in Engineering, 2018(1): 9402836, https://doi.org/10.1155/2018/9402836

[2] Ahmad, K., Hanouf, Z., and Ishak, A. (2017). Mhd casson nanofluid flow past a wedge with newtonian heating. The European Physical Journal Plus, 132(2): 87.

[3] Ahmed, S. and Chamkh, A. J. (2010). Effects of chemical reaction, heat and mass transfer and radiation on mhd flow along a vertical porous wall in the present of induced magnetic field.

[4] Alam, M., Khatun, M. A., Rahman, M., and Vajravelu, K. (2016). Effects of variable fluid properties and thermophoresis on unsteady forced convective boundary layer flow along a permeable stretching/shrinking wedge with variable prandtl and schmidt numbers. International Journal of Mechanical Sciences, 105: 191-205, https://doi.org/10.1016/j.ijmecsci.2015.11.018

[5] Alam, M. J., Murtaza, M. G., Tzirtzilakis, E. E., and Ferdows, M. (2021). Effect of thermal radiation on biomagnetic fluid flow and heat transfer over an unsteady stretching sheet. Computer Assisted Methods in Engineering and Science, 28(2): 81-104.

[6] Ali, K., Alwan, A. A., Bahayan, S., Alhseinat, E., and Ali, M. I. H. (2023). A numerical analysis of the electromagnetic field effect on direct contact membrane distillation performance. Energy Conversion and Management, 292: 117328, https://doi.org/10.1016/j.enconman.2023.117328

[7] Ali, N., Bahman, A. M., Aljuwayhel, N. F., Ebrahim, S. A., Mukherjee, S., and Alsayegh, A. (2021). Carbon-based nanofluids and their advances towards heat transfer applications - a review. Nanomaterials, 11(6): 1628. https://doi.org/10.3390/nano11061628

[8] Aliu, S., Amoo, O., Alao, F. I., and Ajadi, S. (2020). Mechanisms of heat transfer and boundary layers. In Applications of Heat, Mass and Fluid Boundary Layers, pages 23-53. Elsevier. https://doi.org/10.1016/B978-0-12-817949-9.00010-4

[9] Bachok, N., Ishak, A., and Pop, I. (2010). Boundary-layer flow of nanofluids over a moving surface in a flowing fluid. International Journal of Thermal Sciences, 49(9): 1663-1668. https://doi.org/10.1016/j.ijthermalsci.2010.01.026

[10] Brzek, B., Torres-Nieves, S., Lebrón, J., Cal, R., Meneveau, C., and Castillo, L. (2009). Effects of free-stream turbulence on rough surface turbulent boundary layers. Journal of fluid mechanics, 635: 207-243.

[11] Chamkha, A. J. and Issa, C. (2000). Effects of heat generation/absorption and thermophoresis on hydromagnetic flow with heat and mass transfer over a flat surface. International Journal of Numerical Methods for Heat & Fluid Flow, 10(4): 432-449. https://doi.org/10.1017/S0022112009007447

[12] Choudhary, S., Kumar Jarwal, V., Choudhary, P., Loganathan, K., and Pattanaik, B. (2024). Mass-based hybrid nanofluid model for thermal radiation analysis of 78 mhd flow over a wedge embedded in porous medium. Journal of Engineering, 2024(1): 9528362. https://doi.org/10.1155/2024/9528362

[13] Council, N. R., on Engineering, D., Sciences, P., on Physical Sciences, C., Mathematics, Applications, on Physics, B., Committee, P. S., and on the Physics of Plasmas, P. (1986). Plasmas and Fluids. National Academies Press.

[14] El Deeb, S., Al-Harrasi, A., Khan, A., Al-Broumi, M., Al-Thani, G., Alomairi, M., Elumalai, P., Sayed, R. A., and Ibrahim, A. E. (2022). Microscale thermophoresis as a powerful growing analytical technique for the investigation of biomolecular interaction and the determination of binding parameters. Methods and Applications in Fluorescence, 10(4): 042001. https://doi.org/10.1088/2050-6120/ac82a6

[15] Faghri, A., Zhang, Y., and Howell, J. R. (2010). Advanced heat and mass transfer. Global Digital Press.

[16] Gillin, E. J. (2024). Mining knowledge: Nineteenth-century cornish electrical science and the controversies of clay. History of Science, 62(2): 202 – 226. https://doi.org/10.1177/007327532311899

[17] Gireesha, B., Mahanthesh, B., Shivakumara, I., and Eshwarappa, K. (2016). Melting heat transfer in boundary layer stagnation-point flow of nanofluid toward a stretching sheet with induced magnetic field. Engineering science and technology, an international journal, 19(1): 313-321. https://doi.org/10.1016/j.jestch.2015.07.012

[18] Granger, R. A. (1995). Fluid mechanics. Courier Corporation.

[19] Haq, E. U., Khan, S. U., Abbas, T., Smida, K., Hassan, Q. M. U., Ahmad, B., Khan, M. I., Guedri, K., Kumam, P., and Galal, A. M. (2022). Numerical aspects of thermo migrated radiative nanofluid flow towards a moving wedge with combined magnetic force and porous medium. Scientific reports, 12(1): 10120.

[20] Jha, B. K. and Aina, B. (2018). Magnetohydrodynamic natural convection flow in a vertical micro-porous-channel in the presence of induced magnetic field. Communications in Nonlinear Science and Numerical Simulation, 64: 14-34, https://doi.org/10.1016/j.cnsns.2018.04.004

[21] Jimenez, J., Hoyas, S., Simens, M. P., and Mizuno, Y. (2010). Turbulent boundary layers and channels at moderate reynolds numbers. Journal of Fluid Mechanics, 657: 335-360. https://doi.org/10.1017/S0022112010001370

[22] Kakac, S., Yener, Y., and Pramuanjaroenkij, A. (2013). Convective heat transfer. CRC press. 79.

[23] Kituku, N. F. (2018). Influence of inclined magnetic field and thermophoresis on heat and mass transfer wedge flow with variable thermal conductivity. Int. J. Math. Phys. Sci. Res.

[24] Kumar, S. (2022). Basic of thermodynamics. In Thermal Engineering Volume 1, pages 1-93. Springer. https://doi.org/10.1007/978-3-030-67274-4_1

[25] Layton, J. (1967). Application of nuclear power and propulsion technology to solar system exploration. In 3rd Propulsion Joint Specialist Conference, page 512. https://doi.org/10.2514/6.1967-512

[26] Mauri, R. (2023). Heat conduction. In Transport Phenomena in Multiphase Flows, pages 153-170. Springer.

[27] McCormack, P. (2012). Physical fluid dynamics. Elsevier.

[28] Morrison, F. A. (2013). An introduction to fluid mechanics. Cambridge University Press.

[29] Murshed, S. S. and de Castro, C. N. (2016). Conduction and convection heat transfer characteristics of ethylene glycol based nanofluids – a review. Applied energy, 184: 681-695. https://doi.org/10.1016/j.apenergy.2016.11.017

[30] Pandey, A. K. and Kumar, M. (2016). Effect of viscous dissipation and suction/injection on mhd nanofluid flow over a wedge with porous medium and slip. Alexandria Engineering Journal, 55(4): 3115-3123. https://doi.org/10.1016/j.aej.2016.08.018

[31] Petrovi, J., Stamenkovi, Koci, M., Nikodijevi, M., and Bogdanovi-Jovanovi, J. (2018). Mhd flow and heat transfer in porous medium with induced magnetic field effects. Annals of the Faculty of Engineering Hunedoara, 16(1): 171-174. https://doi.org/10.1016/j.proeng.2013.03.156

[32] Rahman, A. M., Alam, M., Alim, M., and Chowdhury, M. (2013). Unsteady mhd forced convective heat and mass transfer flow along a wedge with variable electric conductivity and thermophoresis. Procedia Engineering, 56: 531-537. https://doi.org/10.1016/j.aej.2016.08.018

[33] Ochwach, J. O., Okongo, M. O., & Musundi, S. W. (2018). Modeling the Impact of Soil Porosity on Nitrate Leaching To Groundwater Using the Advection Dispersion Equation. OSR journal.

[34] Sabby, J. A. (2004). A study of binary stars: Absolute properties of the eclipsing binary star RT Coronae Borealis. University of Arkansas.

[35] Sadiq, M. A., Abbas, N., Bahaidarah, H., and Amjad, M. (2023). Unsteady flow and heat transfer of a casson micropolar nanofluid over a curved stretching/shrinking surface. Fluid Dynam. Mater. Process. 19(2). https://doi.org/10.32604/fdmp.2022.021133

[36] Saha, S. J. and Saha, L. K. (2019). Transient mixed convection boundary layer flow of an incompressible fluid past a wedge in presence of magnetic field. Appl. Comput. Math, 8(1): 9-20, 80.

[37] Sarath, K., Osman, M. F., Mukhesh, R., Manu, K., and Deepu, M. (2023). A review of the recent advances in the heat transfer physics in latent heat storage systems. Thermal Science and Engineering Progress, 42: 101886. https://doi.org/10.1016/j.tsep.2023.101886

[38] Jimrise, O., Mark, O., & Ochieng, O. (2022). Mathematical modelling and simulation of nitrate leaching into groundwater. Int J Syst Sci Appl Math, 7, 74-84. https://doi.org/10.11648/j.ijssam.20220704.12

[39] Sarkar, S. and Endalew, M. F. (2019). Effects of melting process on the hydromag netic wedge flow of a casson nanofluid in a porous medium. Boundary Value Problems, 2019: 1-14. https://doi.org/10.1186/s13661-019-1157-5

[40] Sarveshan and and Singh, A. (2015). Magnetohydrodynamic free convection between vertical parallel porous plates in the presence of induced magnetic field. SpringerPlus, 4: 1-13. https://doi.org/10.1186/s40064-015-1097-1

[41] Serth, R. W. and Lestina, T. (2014). Process heat transfer: Principles, applications and rules of thumb. Academic press.

[42] Silu, S. M., Wainaina, M., and Kimathi, M. (2018). Effects of magnetic induction on mhd boundary layer flow of dusty fluid over a stretching sheet. Glob J Pure Appl Math, 14: 1197-1215.

[43] Singh, H. and Myong, R. S. (2018). Critical review of fluid flow physics at micro to nano-scale porous media applications in the energy sector. Advances in Materials Science and Engineering, 2018(1): 9565240. https://doi.org/10.1155/2018/9565240

[44] Sorensen, C. (2021). Magnetohydrodynamic Heat Transfer for Fusion Energy. PhD thesis, Massachusetts Institute of Technology.

[45] Tulu, A. and Ibrahim, W. (2019). Magnetohydrodynamic boundary layer flow of nanofluid past a wedge embedded in a porous medium. In Proceeding of the Third International Research Symposium.

[46] Uddin, M., Kabir, M., Bég, O. A., and Alginahi, Y. (2018). Chebyshev collocation computation of magneto-bioconvection nanofluid flow over a wedge with multiple slips and magnetic induction. Proceedings of the Institution of Mechanical Engineers, Part N: Journal of Nanomaterials, Nanoengineering and Nanosystems, 232(4): 109-122. https://doi.org/10.1177/2397791418809795

[47] Ullah, I., Shafie, S., and Khan, I. (2018). Heat generation and absorption in mhd flow of casson fluid past a stretching wedge with viscous dissipation and newtonian heating. Jurnal Teknologi, 80(3). https://doi.org/10.11113/jt.v80.11138

[48] White, F. M. and Majdalani, J. (2006). Viscous fluid flow, volume 3. McGraw-Hill New York.

[49] Zhang, Z., Guan, S., Wu, R., and Zhao, C. (2024). Examination of two-phase behaviors in porous media during pool boiling. Science China Technological Sciences, pages 1-19. https://doi.org/10.1007/s11431-023-2525-8

[50] Zhu, J. and Cao, J. (2019). Effects of nanolayer and second order slip on unsteady nanofluid flow past a wedge. Mathematics, 7(11): 1043. https://doi.org/10.3390/math7111043

[51] Percy, S., Knight, C., McGarry, S., Post, A., Moore, T., and Cavanagh, K. (2014). Thermal energy harvesting for application at MEMS scale. Springer.